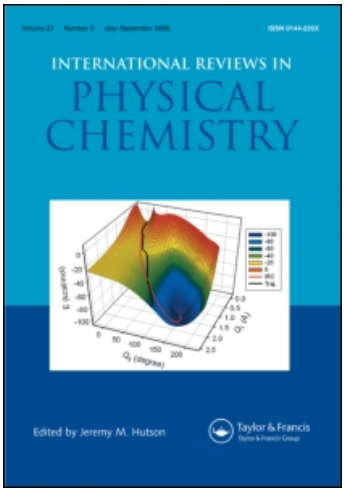

International Reviews in Physical Chemistry
Publication details, including instructions for authors and subscription information:
http://www.informaworld.com/smpp/title~content=t713724383

The kinetics of phase transitions observed by energy-dispersive X-ray diffraction

Ruggero Caminiti; Valerio Rossi Albertini

Online publication date: 26 November 2010

To cite this Article Caminiti, Ruggero and Albertini, Valerio Rossi(1999) 'The kinetics of phase transitions observed by energy-dispersive X-ray diffraction', International Reviews in Physical Chemistry, 18: 2, 263 — 299
To link to this Article: DOI: 10.1080/014423599229965
URL: http://dx.doi.org/10.1080/014423599229965

INTERNATIONAL REVIEWS IN PHYSICAL CHEMISTRY, 1999, VOL. 18, NO. 2, 263–299

The kinetics of phase transitions observed by energy-dispersive X-ray diffraction

RUGGERO CAMINITI†

Dipartimento di Chimica, Istituto Nazionale per la Fisica della Materia, Università 'La Sapienza', Piazzalle Aldo Moro 5, 00185 Rome, Italy

and VALERIO ROSSI ALBERTINI‡

Istituto di Struttura della Materia del Consiglio delle Ricerche Nazionale, Area della ricerca di Tor Vergata, Via del fosso del Cavaliere 100, 00133 Rome, Italy

A new energy-dispersive X-ray diffraction (EDXD) method to study the kinetics of the phase transitions (PTs) is reviewed. It enables one to follow the evolution of systems undergoing structural transformations in real time. It is based on a novel approach to PTs and provides several advantages with respect to the conventional techniques used for the same purpose. A detailed treatment of the theory is accomplished to demonstrate the consistency and reliability of this method. Despite the initial complexity of the subject that involves the interactions between X-ray and matter, just very simple measurements are required. Furthermore, the data processing is trivial and the relevant information on the PTs can be straightforwardly obtained from the X-ray spectra. The applications of the EDXD–PT method to the systems studied until now, namely polymeric, biological and mineralogical samples, are finally reported.

1. Introduction

Information about the atomic structure of a sample can be gained by observing the modulation of the intensity spectrum of a probe whose wavelength is comparable with the interatomic distances. If the probe is electromagnetic radiation, the wavelength is in the X-ray range.

The X-ray diffraction theory due to Thomson and Debye describes this modulation of the probe intensity spectrum, which arises because of interaction with the sample, as the effect of coherent superposition of waves elastically scattered by atomic core electrons. This kind of approach is completely classic [1]. The electrons are regarded as small antennae scattering with a dipolar distribution. Nevertheless, it is sufficient to explain the features and the characteristics of diffraction patterns and to obtain the structural information required. Quantum effects at these energies are still small and can be considered as perturbations. They can be taken into account by introducing some suitable corrections connected to the inelastic contribution to the scattering because of the outer shell electrons, that is the Compton effect.

The elastic contribution to the scattering is a function of the momentum $\Delta\mathbf{p}$ exchanged by the radiation with the atomic tightly bound electrons. For a generic system, $\Delta\mathbf{p}$ is a vectorial quantity, having three components, and measurements of the intensity must be carried out by observing in turn each of them. However, if isotropic

† Email: r.caminiti@caspur.it.
‡ Email: valerio@dns.ism.rm.cnr.it.

International Reviews in Physical Chemistry ISSN 0144–235X print/ISSN 1366–591X online © 1999 Taylor & Francis Ltd
http://www.tandf.co.uk/JNLS/rpc.htm http://www.taylorandfrancis.com/JNLS/rpc.htm

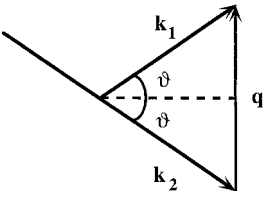

Figure 1. Diagram of the momentum transfer.

systems are investigated, the diffracted intensity depends only on the modulus of $\Delta\mathbf{p}$ and not on its orientation. In this case a scalar quantity q can be defined, called the *scattering parameter* [2], which represents the modulus of $\Delta\mathbf{p}$ expressed in $\hbar$ units. Diffraction patterns produced by disordered samples can be drawn by plotting the scattered intensity as a function of the free parameter q only.

In figure 1 the relation between q and the experimental quantities is shown:

$$q = 2k \sin \vartheta, \tag{1}$$

2ϑ being the total scattering angle and k the modulus of both wave-vectors $\mathbf{k}_1$ and $\mathbf{k}_2$ of the incident and scattered radiation [3] respectively. In fact, since the scattering is elastic, the energy E of the radiation remains unchanged during the scattering. Moreover, according to the dispersion relation of an electromagnetic radiation $E = n\hbar ck$, where n is the refraction index and c is the speed of light, the modulus of its wave-vector (wavenumber) is proportional to its energy. Therefore, in the hypothesis of elastic scattering, the wave-vector of radiation interacting with a sample can vary its direction but not its modulus, that is the X-ray beam can be deflected but it maintains its wavelength unchanged. As E is proportional to k (equation (1)), the following equation holds:

$$q(E, \vartheta) = \alpha E \sin \vartheta, \tag{2}$$

where α is a constant (equal to $2/\hbar c = 1.014$ Å^{-1} keV^{-1}) in the approximation that n at the typical energies of X-rays is always unity, regardless of the material forming the sample (usually $1 - n = 10^{-6}$, as an order of magnitude). The preceding relation is another way of expressing the well known relation $q = (4\pi/\lambda) \sin \vartheta$, where λ is the radiation wavelength.

This concise introduction to X-ray diffraction of disordered systems is sufficient for understanding the following subjects. Two methods are available to perform a scan of q and to draw the scattered intensity profile as a function of it.

(1) The first is to use a monochromatic beam (E fixed), for instance a fluorescence line produced by a laboratory X-ray tube, and to make an angular scan (angle-dispersive X-ray diffraction (ADXD)),
(2) The second consists in utilizing a continuous spectrum radiation, often called *white* by analogy with the visible light, for example the Bremmstrahlung of the same X-ray tube, the scattering angle being fixed (energy-dispersive X-ray diffraction (EDXD)).

The first alternative is the conventional method and the distinction between the two methods was made at the end of the 1960s [4, 5]. In fact, although the second possibility has been known for a long time, only in this period have solid-state detectors with an acceptable resolution appeared, enabling the construction of a new kind of diffractometer.

2. Why is energy-dispersive X-ray diffraction used on disordered systems?

It is worth comparing EDXD with the usual ADXD, in order to illustrate its qualities and defects. The merits can be summarized as follows [6, 7].

(1) *Reduction in the acquisition time.* We can estimate the time saving by considering that the diffracted intensity is proportional to that of the primary X-ray beam. The intensity concentrated in the fluorescence line (in ADXD) is, in typical working conditions, from one to two orders of magnitude lower than the intensity distributed in the entire continuous spectrum (in EDXD). Therefore, this is also, roughly, the ratio between the acquisition times in the two cases.

(2) *Steady apparatus during data collection.* This simplifies the experimental procedure, since the beam trajectory is fixed. Hence, also very small samples can be used. In fact, unlike ADXD, no movements may compromise the alignment, inducing systematic errors. Furthermore, complex and cumbersome devices can be installed, as high-pressure or variable-temperature cells, even if the path to the sample is very narrow; it must be just a little wider than the transverse section of the X-ray beam.

(3) *Parallel collection of the spectrum points.* In the ADXD method, spectrum points are collected in a sequential way, with a scanning rate proportional to the angular speed of the diffractometer arms. In contrast, EDXD permits multiplex acquisition; the points are collected simultaneously at each value of q (or E; see equation (2)).

On the other hand a few defects must be noticed.

(4) *Complication of experimental data processing.* This arises because both the scattered intensity and the other quantities involved in a diffraction measurement depend on the energy of the radiation. Therefore a separate treatment of each energy component is required.

(5) *Need to join various X-ray spectra.* According to equation (1) at a given angle, using a radiation having a continuous energy spectrum in the interval (E_1, E_2), the accessible q range in the reciprocal space is

$$\Delta q(\vartheta) = q_2 - q_1 = \alpha(E_2 - E_1)\sin\vartheta. \tag{3}$$

In figure 2 the q ranges scanned at various angles, according to equation (3), are shown. To cover the widest possible region of q space, several measurements performed in correspondence to a set of scattering angles are needed. The spectra must then be connected to reconstruct the whole diffraction pattern.

(6) *Decrease in the q resolution.* Starting from equation (2), we can approximate the relative error on q by calculating its logarithmic derivative.

$$\frac{\Delta q}{q} \approx \frac{\Delta E}{E} + \cot\vartheta\,\Delta\vartheta. \tag{4}$$

The relative q resolution is composed of two parts. The first contribution is due to the energy resolution of the detector and of its electronic chain, and the second to the angular divergence of the X-ray beam. In ADXD, only the latter is present. Furthermore, while the angular term can be adjusted by changing

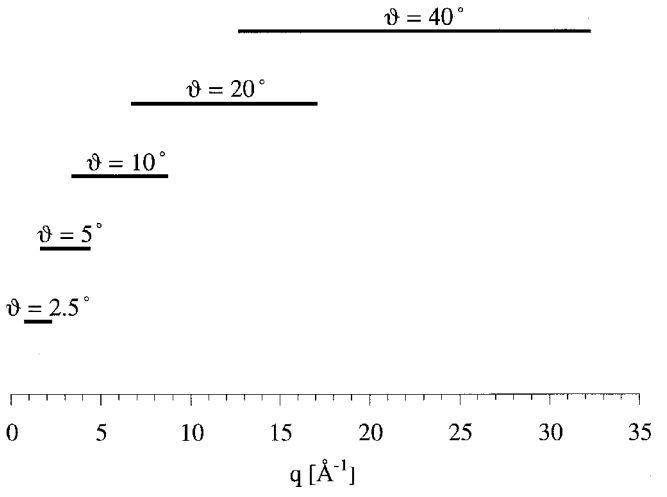

Figure 2. q range accessible at various angles using a white X-ray beam with components up to 50 keV.

the width of the collimation slits, the energy term is fixed. This is one reason why EDXD is particularly suitable for disordered systems (amorphous solids, liquids and gases). They do not produce a drastic modulation of the incident spectrum like crystalline samples do (Bragg peaks). The broad oscillations of the diffraction patterns are not influenced very much by the instrumental transfer function and the deconvolution does not require precise and complicated mathematical models.

In section 7.3 we shall show that our technique is based on the fact that the advantages (1)–(3) of EDXD are used in a determinant way, while the drawbacks (4)–(6) are completely overcome.

3. Instrumentation

An energy-dispersive X-ray diffractometer is similar, from the geometric point of view, to an angle-dispersive diffractometer without regard to the particular scattering configuration adopted. The difference concerns the detector and monochromators (the latter in energy dispersion are absent). Figure 3 shows a schematic picture of an energy-dispersive X-ray diffractometer [8].

In the following section a brief overview of the three fundamental components of the apparatus is shown to introduce the experimental technique.

3.1. *The source*

An ordinary X-ray generator can be utilized as the radiation source [7]. A typical spectrum produced by a hot-cathode tungsten target tube is shown in figure 4. In it, the two characteristic features of the fluorescence lines and of the continuous Bremmstrahlung hunch can be recognized. The first is produced by the de-excitation of tungsten atoms when ionized by the fast electron beam impinging on the target. The emission is quantized, being the effect of a transition between stationary atomic states, and the lines appear at certain characteristic energies. On the contrary, Bremmstrahlung (braking radiation) is not a quantized phenomenon for it is due to a deceleration of the incident fast electrons subjected to the electrostatic potentials

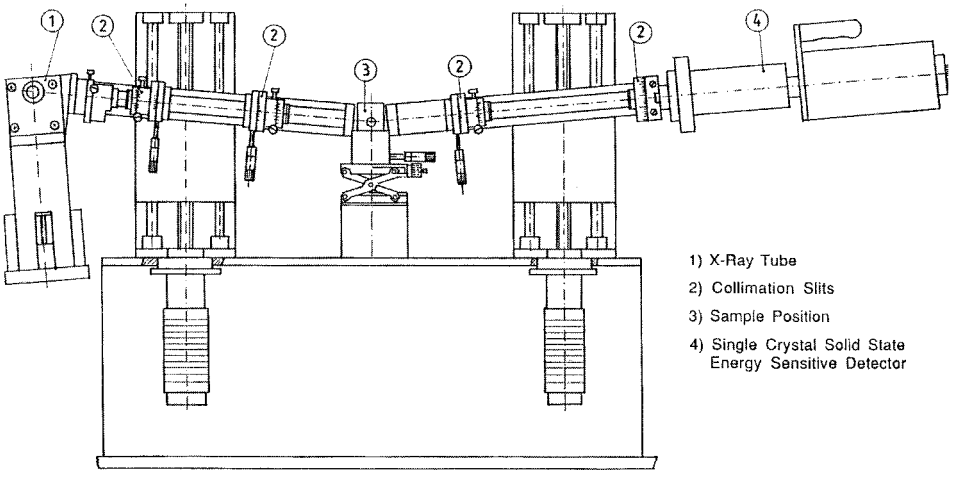

Figure 3. Schematic view of the experimental apparatus.

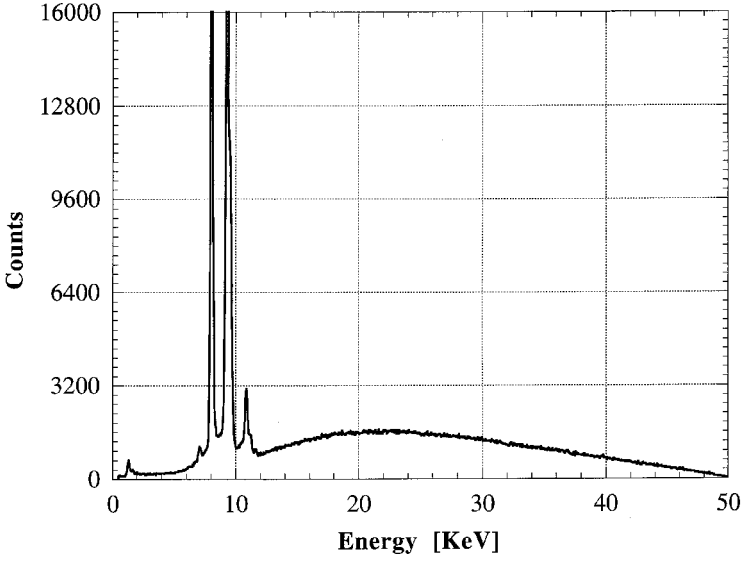

Figure 4. X-ray beam produced by a tungsten anode like that used for these measurements.

inside the tungsten crystalline lattice. The deceleration produces, according to classical electrodynamical laws, the emission of radiation [3]. Since the braking depends on non-quantized variables (the direction of the electrons with respect to the symmetry axes of the tungsten lattice, their minimum distance from the lattice charges, their speed, etc.), the energy of the emitted radiation ranges from zero (undisturbed electron motion) to the whole kinetic energy of the electrons (for those that are completely stopped in a single collision).

In ADXD, Bremmstrahlung must be removed from the primary beam or, at least, reduced as much as possible by filtering or by monochromation. In EDXD, the fluorescence lines are not a problem and the entire spectrum is used. The monochromator in ADXD has two opposite effects. On the one hand, it reduces the X-ray intensity because of poor reflection efficiency. On the other hand its second

stage, that is the crystal between the sample and the detector, cuts the Compton line (section 4.1) contained in the scattered beam. In contrast, in EDXD all the energy components must be collected and, at each energy E, there are two contributions to the intensity: the first is due to the elastic scattering of an X-ray having an initial energy E and the second to the inelastic scattering of an X-ray having an initial energy E', which exceeds E by the amount that equals the Compton shift. Consequently, the Compton intensity cannot be either suppressed or measured and usually it is subtracted by theoretically calculating its contribution to the total scattered intensity.

3.2. *The detector*

The detector is the most important element of an energy-dispersive diffractometer; it is a real improvement with respect to the angle-dispersive machines. To understand the essence of the EDXD technique, which is a mixing of spectrometry and diffractometry, it is worth giving a short explanation about how this type of detector (solid-state detector (SSD)) works.

The sensitive part of the SSD is a semiconducting (silicon or germanium) single crystal. Atoms of another suitable element, for example lithium, are inserted in the crystal by diffusion, in order to create inside it a p–n junction. Thus the crystal behaves as a diode and can be directly polarized by applying a voltage at its extremities. If an ionization agent, namely a perturbation with energy sufficient to break chemical bounds, comes inside the crystal, the ejected electrons go to the conduction band and are available for charge transfer. At the same time, an equal number of positive charges appear in the valence band, because the remaining electrons can no longer completely screen the positive ions. These changes in the valence band are called holes and can carry the electrical current as well. When a photon of a certain wavelength penetrates the crystal and is absorbed, many different mechanisms of excitation, having different energies, are activated in the lattice. Nevertheless, the final result is a redistribution of the energy from the higher-energy excitations to the lowest-energy excitations, that is electron–hole pair creation. Soon after the pairs are created, they are pushed by the external voltage and separated into electrons and holes moving in opposite directions. When they reach the Ohmic contacts, a current pulse is recorded. The integral over time of this pulse gives the total charge and, therefore, the number of electron–hole pairs. The product of this number by the energy needed for the creation of each pair equals the energy of the absorbed photon. Finally, this information is sent to a computer containing a multichannel analyser (MCA) card (section 3.3).

3.3. *The multichannel analyser*

The working of this device can be schematically represented as a frequency histogram. The horizontal axis corresponds to the energy and is divided into discrete intervals (channels) labelled by integer indices. The average value of energy in each interval is a linear function of the index of that interval. The vertical axis is also divided in integer units. When a photon of a given energy E is detected by the SSD, a pulse passes the information on the event through the electronic chain connecting it to the MCA. The MCA increases by unity the integer value corresponding to the channel inside which E is contained. In this way, a digital reconstruction of the energy spectrum of the scattered radiation is accomplished. To find the correspondence between the channel indices and the energies, that is to calculate the coefficient of the above-mentioned linear relation, preliminary calibration measurements have to be made.

4. Scattering and concomitant phenomena

The maximum part of the intensity reaching the detector after the interaction of the X-ray primary beam with the sample is due to single elastic scattering. The elastically scattered photons show well defined phase differences induced by the position of the scattering atoms and, as an effect of this phase coherence, they interfere with each other [3]. The intensity I_{coh} of the single scattered radiation is composed of three terms. The first corresponds to the independent scattering of the atoms and exhibits no modulations. The second corresponds to the interference of radiation scattered by atoms belonging to the same local unity (molecules or small domains into which the sample is divided) and the third corresponds to different units. The latter two contributions are together called the 'coherent dependent intensity' and they contain information on the arrangement of atoms in the sample.

However, for correct interpretation of diffraction spectra, other phenomena must also be considered [9]. Usually, for thin samples, multiple scattering can be neglected. Multiple scattering occurs when a photon scattered in some direction is scattered again, being deflected into the solid angle of acceptance of the detector. X-ray absorption, especially of lower-energy components, and inelastic scattering must be taken into account.

4.1. *Inelastic X-ray scattering: Compton effect*

When the energy of the photons increases, so that their momentum approaches mc (m is the electron rest mass), the quantum nature of the interaction appears. The phenomenon can be suitably described by Compton's model in which scattering is regarded as a collision between two material points. During the impact, the photon gives part of its energy to the electron and is scattered with a longer wavelength.

Defining by E' and E the energies of the photon before and after the collision respectively, $\Delta E = E' - E$ can be expressed as follows [7]:

$$\Delta E = \frac{2E^2 \sin^2 \vartheta}{mc^2} \frac{1}{1 - (2E/mc^2) \sin^2 \vartheta}. \tag{5}$$

Therefore, photons collected at energy E may have reached the detector in two ways: after either elastic or inelastic scattering. They give the two contributions mentioned in section 3.1.

Since in ADXD, single-energy radiation is used, inelastic scattered photons can be eliminated by monochromation. In EDXD these photons are indistinguishable from the others and their contribution can be subtracted only by theoretical calculation.

4.2. *X-ray absorption*

Although the capability of X-rays in penetrating matter is probably their most notable property, yet a part of them (sometimes not small) is absorbed by the substances through which they pass. In the energy range of X-rays suitable for diffraction, two effects produce the intensity reduction: the 'true' or photoelectric absorption, occurring when the photon disappears inducing the ionization of a core electron, and the 'equivalent' extinction, when the photon is scattered outside the solid angle subtended by the detector slits.

The total absorption A (true plus equivalent) of an X-ray beam impinging

perpendicularly on the flat surface of a homogeneous sample is described according to the Lambert–Beer law:

$$I_T(E,x) = I_0(E)\exp\left(-\frac{\mu}{\rho}\rho x\right) \tag{6a}$$

and

$$A(E,x) = \frac{I_T(E,x)}{I_0(E)} \tag{6b}$$

where

$$\frac{\mu}{\rho}(Z,E) = \left(\frac{\mu}{\rho}\right)_P + \left(\frac{\mu}{\rho}\right)_S$$

is the mass absorption coefficient, dependent on the chemical species (on the atomic number Z) and on the energy; the two terms into which μ/ρ is divided are photoelectric and scattering (Thomson +Compton) contributions. I_0 is the incident intensity (whose spectrum is shown in figure 4) and I_T is the fraction of I_0 that is transmitted at a depth x below the sample surface. ρ is the mass density of the sample. In the equation for I_T, the ρ dependence of μ is rendered explicit because variable-density systems will also be considered [9].

5. Equation for the diffractometer

To obtain the equation describing the real behaviour of the diffractometer, the theoretical principles must be suitably adapted. This equation connects the spectral intensity of X-rays observed at the detector with the quantities that contribute to produce it.

We start by calculating the X-ray absorption along the optical path of the beam inside a sample having a parallelepipedal shape for both elastic and inelastic scattering. In the following treatment, the X-ray absorption is called 'coherent' if calculated along a path in which an elastic Thomson scattering occurs, and 'incoherent' if the scattering is inelastic. In transmission geometry, the coherent absorption is given by the following equation:

$$A_{coh}(E,\vartheta) = \exp\left(-\frac{\mu}{\rho}\rho t\sec\vartheta\right), \tag{7}$$

where the optical path $t\sec\vartheta = x_1 + x_2$ is independent of the scattering point, as can be seen in figure 5. For inelastic scattering, the photon energy before the deflection is E' and it is E afterwards.

The absorption coefficients before and after the scattering point (placed at x) are respectively

$$A_1(E',\vartheta,x) = \exp\left(-\frac{\mu}{\rho}(E')\rho x\sec\vartheta\right) \tag{8a}$$

and

$$A_2(E,\vartheta,x) = \exp\left(-\frac{\mu}{\rho}(E)\rho(t-x)\sec\vartheta\right) \tag{8b}$$

The total absorption in the sample is

$$A(E,E',\vartheta,x) = \exp\left[-\left(\frac{\mu}{\rho}(E')x + \frac{\mu}{\rho}(E)(t-x)\right)\rho\sec\vartheta\right]. \tag{9}$$

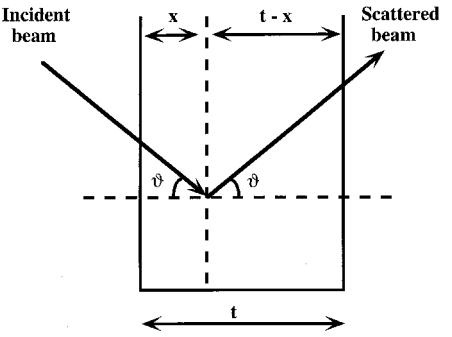

Figure 5. Symmetrical transmission geometry utilized for X-ray diffraction measurements. This configuration minimizes the data refinement because all optical paths in the sample have the same length regardless of the depth x of the scattering point from the surface.

Since the scattering probability is uniform along the optical path as the sample is homogeneous, the reduction in the intensity caused by inelastic absorption is the average over t of this function. The integral can be calculated exactly:

$$A_{\text{inc}}(E, E', \vartheta) = \langle A(E, E', \vartheta, x)\rangle_t = \frac{\exp[-(\mu/\rho)(E')\rho t \sec\vartheta] - \exp[-(\mu/\rho)(E)\rho t \sec\vartheta]}{[(\mu/\rho)(E) - (\mu/\rho)(E')]\rho t \sec\vartheta}. \quad (10)$$

The inelastic term must be completed by introducing a factor that derives from quantum theory. This is the only modification to the classical model necessary to reproduce the experimental data correctly. The correction depends on the fact that the electrons involved in the scattering are not free, as assumed in Compton's treatment [10]. The factor is E'/E. The moment distribution of the electrons, which modifies the Compton shift (equation (5)), can be completely neglected.

Let $I_{\text{inc}}(E', \vartheta)$ be the total intensity of X-rays inelastically scattered by the sample. It is the equivalent of $I_{\text{coh}}(E, \vartheta)$ in the case of inelastic scattering. It has the same coefficients but is calculated corresponding to the initial photon energy E'. The main difference with respect to $I_{\text{coh}}(E, \vartheta)$ is that $I_{\text{inc}}(E', \vartheta)$ has no interference modulation. So, it can be obtained *a priori* by summing all the intensities inelastically scattered by each atom or, alternatively, m times the intensity scattered by a single stoichiometric unit (m is the number of units).

In the single-scattering approximation (photons that are elastically or inelastically scattered once cannot be scattered again) the intensity detected at a distance R from the sample is

$$I_{\text{scatt}}(E, E', \vartheta) = \left(\frac{r_0}{R}\right)^2 [I_0(E) P(E, \vartheta) A_{\text{coh}}(E, \vartheta) I_{\text{coh}}(E, \vartheta) + \frac{E'}{E} I_0(E') P(E', \vartheta) A_{\text{inc}}(E, E', \vartheta) I_{\text{inc}}(E', \vartheta)], \quad (11)$$

where I_0 is the intensity of the primary beam as a function of energy (intensity spectrum) and P the polarization of the scattered beam.

However, this is still a theoretical equation and it must be still adapted to the characteristics of the instrument. The intensity I_{obs} observed by the detector is proportional to I_{scatt} through a constant K, which is different for each scattering angle.

K contains the factor $(r_0/R)^2$ and all the quantities that modify the total photon flux at the detector (the X-ray tube-to-sample distance, the sample-to-detector distance, the positions of the collimation slits and the surfaces that they delimit, etc.).

Furthermore, if the sample is not a solid, another modification is required to consider the presence of the holder. Let us consider the intensity I_{obs} scattered by a cell filled with the sample (sample +cell system S) and the intensity I_{emp} scattered by the empty cell in the same conditions. The aim is to express the effect of the presence of the cell in the overall intensity I_{obs} in terms of I_{emp}. In this way the contribution due to only the sample can be isolated. The calculations lead [7] to the following equation for I_{obs}:

$$\begin{aligned} I_{obs}(E, E', \vartheta) = {} & K A_{coh}^{cel}(E, \vartheta)[I_0(E) P(E, \vartheta) A_{coh}^{sam}(E, \vartheta) I_{coh}(E, \vartheta) \\ & + \frac{E'}{E} I_0(E') P(E', \vartheta) A_{inc}^{sam}(E, E', \vartheta) I_{inc}(E', \vartheta)] \\ & + A_{coh}^{sam}(E, \vartheta) I_{emp}(E, E', \vartheta), \end{aligned} \tag{12}$$

in which A is the absorption, the superscripts sam and cel correspond to sample and cell respectively, and the subscripts coh and inc denote coherent and incoherent scattering respectively.

6. Experimental data processing and refinement

A number of corrections are usually required for the refinement of experimental data in order to isolate the structural information contained in them. This processing involves also unknown quantities that must be measured either by other X-ray measurements or by theoretical calculations.

Schematically the corrections can be divided into two classes: firstly corrections due to the effects induced by instrumentation; secondly corrections due to the effects induced by samples.

Corrections included in the first class are as follows:

(i) for the X-ray source,
  (*a*) normalization to the incident white spectrum;
  (*b*) normalization to the polarization of the primary beam;
(ii) for the collimation system, deconvolution for the angular divergence;
(iii) for the detector,
  (*a*) deconvolution for the finite energy resolution;
  (*b*) elimination of the escape peaks.

Corrections included in the second class are as follows:

(i) normalization to sample absorption;
(ii) elimination of Compton single-scattering and possible fluorescence contributions.

In the previous list, all factors that modify the quantity of interest in the observed intensity, namely I_{coh}, are divided from the point of view of the objects producing them. Three more effects are mentioned which are omitted in equation (12), to avoid unnecessary complications in the mathematical formalism. These effects are the corrections for escape peaks, for fluorescence lines and for the convolution of the signal with the instrument transfer function. Therefore, I_{obs} must be considered as if disturbances due to these phenomena have already been eliminated.

However, as will be shown in section 7.3 the technique which consists in using

EDXD to observe the kinetics of the phase transitions, is not affected by the majority of these problems. The only corrections that must be made concern the escape peaks (which are unavoidable as they are an intrinsic effect of the detector crystal), elimination of the fluorescence peaks (if any) from the scattered radiation intensity (not included in equation (12)), and X-ray absorption of the sample (which must be measured to normalize the diffraction spectra as discussed in section 7.2). Therefore we shall discuss the characteristics of just these three phenomena.

6.1. *Escape peaks*

The sensitive part of a SSD is a pure germanium crystal, which is almost opaque to the incoming X-ray beam.

When a photon of energy E_0 is absorbed by an atom of germanium owing to fluorescence (section 4.2; true absorption), another photon of energy E_f is emitted. Since the mean free path of the latter is very long in the material that produced it, the fluorescence photon has an appreciable probability of escaping outside the crystal. If this happens, the detector reveals the original photon not at E_0, but at a lower energy $E_0 - E_f$, because of the loss of E_f subtracted by the escaped photon. Furthermore, the escape probability varies with E_0. To determine this probability, a preliminary calibration is required. It consists in measuring a spectrum composed of isolated lines at various energies and calculating the ratio R of the height of each line to the height of the corresponding escape peaks. Fitting the plot of R suitably as a function of energy, the ratios are known at any energy [7].

6.2. *Fluorescence lines*

In addition to scattering, samples irradiated by X-rays can produce fluorescence radiation like the semiconducting crystal in the preceding paragraph. The fluorescence lines are detected and superimposed on the pure diffraction spectrum. If there were no re-emission after the absorption, the only effect would be the decrease in the scattered intensity (see the following section), which is also considered later. Owing to the re-emission, additive contributions represented by extra intensities at the characteristic energies appear. They can be removed, for example, by suitable fits of the lines, without further modifications of the other parts of the spectrum.

6.3. *Absorption*

With reference to section 4.2, to compensate for the intensity decrease due to elastic and inelastic absorption, the coefficients μ must be measured. The effect of absorption on a X-ray beam passing through a sample is shown in figure 6 as a function of energy.

If the sample is not contained in a holder, only two measurements are required; otherwise three are necessary, under the same conditions. The diffractometer arms are placed in the direct transmission ($\vartheta = 0^\circ$). In the most general case the three measurements concern firstly the empty cell, secondly the filled cell and thirdly the white beam of intensity $I_0(E)$. Equations describing the observed intensities for the empty cell and the filled cell respectively are, according to equation (6),

$$I_1(E) = I_0(E)\exp[-\mu_1(E)t_1], \tag{13}$$

$$I_2(E) = I_0(E)\exp\{-[\mu_1(E)t_1 + \mu_2(E)t_2]\}, \tag{14}$$

in which t_1 and t_2, μ_1 and μ_2 are the (known) thicknesses and the absorption coefficients of the cell and the sample respectively. In the equations, E' does not appear since the Compton shift vanishes at zero angle.

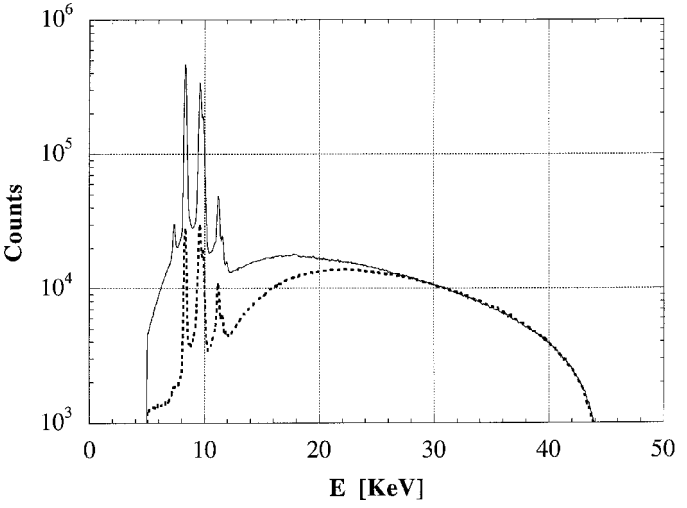

Figure 6. White incident X-ray beam produced by a tungsten tube (——) and after being transmitted through the sample (– – – –). The energy components below 20 keV are intensely absorbed. The logarithmic scale allows us to evaluate better the reduction in the intensity. (Reprinted with permission from [12]; copyright 1997 by Marcel Dekker, Inc.)

From I_0 and these two equations, μ_1 and μ_2 are easily derived. This time it is not relevant whether I_0 is not the real spectrum of the incident radiation because it appears in all the relations and can be eliminated, therefore not influencing the calculation of μ_1 and μ_2.

7. Kinetics of the phase transitions

EDXD is a powerful technique for studying systems undergoing phase transitions (PTs). Under a very general hypothesis a transition coordinate can be defined in analogy to the reaction coordinate in chemical transformations. The time evolution of this coordinate enables one to follow the change in the system. We shall distinguish between constant-density phase transitions (CDTs) from the variable-density phase transitions (VDTs), although the former are just a particular case of the latter. The separate treatments are useful because in CDTs the properties and limits of this method can be shown more clearly.

7.1. *Constant-density phase transitions*

From now on, the subscripts 1 and 2 will indicate quantities related to the first or to the second phase component respectively. We temporarily neglect the sample holder contribution. This simplifies the treatment. We shall show later that its presence does not influence the determination of x.

Equation (12) can be written as [11]

$$I_{\text{obs}}(E, E', \vartheta) = KI_0(E)\,P(E, \vartheta)\,A_{\text{coh}}^{\text{sam}}(E, \vartheta)\left(I_{\text{coh}}(E, \vartheta) + \frac{E' I_0(E')\,P(E', \vartheta)\,A_{\text{inc}}^{\text{sam}}(E, E', \vartheta)}{E I_0(E)\,P(E, \vartheta)\,A_{\text{coh}}^{\text{sam}}(E, \vartheta)} I_{\text{inc}}(E', \vartheta)\right). \tag{15}$$

Given a sample undergoing a PT, the expression inside the large parentheses is called I_1, if the system is in the first phase, and I_2, if it is the second phase. The change in this

expression during the transition is due to $I_{coh}(E, \vartheta)$, which depends on the phase, being a function of the geometrical arrangement of the constituent atoms. However, neither the self-scattering part nor the $I_{inc}(E', \vartheta)$ term vary because they depend only on the type and number of scattering atoms, which remain unchanged in the CDT.

We define N_1 as the number of stoichiometric units in the first phase, N_2 as the number in the second phase and $x = N_1/(N_1 + N_2)$ (second-phase concentration). For the total scattered radiation of intensity $I(x)$ connected with a certain value x (omitting the dependence on ϑ and E), the following relation holds:

$$I(x) = (1 - x) I_1 + x I_2. \tag{16}$$

For this equation (demonstrated later in the general VDT case) to be true, the following conditions are to be met.

(*a*) The stoichiometry must not change during the transition.

(*b*) The domains in each phase must have dimensions such that the intradomain coherent scattered intensity shows the same spectral profile of a macroscopic object having an identical structure. In other terms, the change in the scattered radiation spectrum due to the termination of the structure at the surface must be negligible. In fact, if the domains were too small, the superposition of the coherently scattered waves (as in the case of interference among a few sources) would have different characteristics with respect to the diffraction of a large object. Therefore, the linear relation (16) would no longer be valid, since in the expression for I_1 and I_2 the contributions due to the intradomain interference would not remain constant during the transition.

(*c*) The radiation coherently scattered by domains must not interfere with each other. When this happens, deviations from linearity are expected again. This condition holds more strongly, the larger the distance between the atom pairs of two different domains, and the less the reciprocal position of the two domains is fixed. In fact, interference phenomena are strongly depressed by a wide distribution of possible positions (as in the case of a low-pressure gas that does not induce modulations in the spectrum of an X-ray beam scattered by it).

To render explicit the time dependence of x, we can call $I_{obs}(t)$ the spectrum collected at t. As the theoretical forms of I_1 and I_2 are unknown, measurements corresponding to $x = 0$ and $x = 1$ values have to be utilized, that is equation (15): $I_{obs\,1} = K I_0 P A I_1$ and $I_{obs\,2} = K I_0 P A I_2$, where the subscript coh for A has been omitted. Since A depends only on the density [11], once the stoichiometry of the sample is fixed, A is the same in both equations. In the same way, K, I_0 and P do not vary, because the experimental parameters remain unchanged; thus, we have

$$x(t) = \frac{I_{obs}(t) - I_{obs\,1}}{I_{obs\,2} - I_{obs\,1}}. \tag{17}$$

In fact, x, at a fixed ϑ, is a function of E, that is of the channel index j, since E and j are linked by a linear relation (section 3.3). It would be possible to obtain $x(t)$ by applying equation (17) directly to the total diffracted intensity recorded at ϑ but it is more useful to calculate the distribution of the $x(t, j)$ at a given t. In fact, in the former case, only the mean x value is obtained while, in the latter case, a statistical treatment

can be applied to the $x(t, j)$ distribution as a function of j. The consistency of the results will be an indication of the reliability of this method and the correctness of the hypothesis. Furthermore, in many cases, the total intensity diffracted in the q interval scanned at ϑ according to equation (3) remains almost unchanged. This happens when, during the PT, the diffracted radiation changes its spectral profile but not the area subtended by it. In such an event just the second (differential) procedure can provide $x(t)$.

7.2. *Extension to the variable-density case*

We define $\rho_1 = \rho(x = 0)$ as the first-phase density and $\rho_2 = \rho(x = 1)$ as the second-phase density. During the transition from the first to the second phase, the total volume of the sample changes according to the variation in density. We assume that the total volume is additive, that is it is just the sum of volumes occupied by the two phases. By definition of the transition coordinate, at a certain value of x, the total volume is

$$V(x) = \frac{N_1}{\rho_1} + \frac{N_2}{\rho_2} = N\left(\frac{1-x}{\rho_1} + \frac{x}{\rho_2}\right). \tag{18}$$

Leaving unchanged the experimental conditions of the diffractometer (namely the scattering angle, the slit width and the distances) the scattering volume v (the irradiated volume of the sample) remains constant. Also, assuming that the composition inside the scattering volume is the same over the whole volume, the number of scattering centres (stoichiometric units in the two different phases of the system) in v is $n(x) = n_1(x) + n_2(x)$, with $n_i/\mathrm{v} = N_i(x)/V(x)$, $i = 1, 2$:

$$n_1(x) = \mathrm{v}\frac{(1-x)N}{[(1-x)/\rho_1 + x/\rho_2]N} \tag{19a}$$

and

$$n_2(x) = \mathrm{v}\frac{xN}{[(1-x)/\rho_1 + x/\rho_2]N}. \tag{19b}$$

I_{inc} depends on x only through the number of scattering centres, but its coefficient in equation (15), or rather $A_{\mathrm{inc}}(E', \vartheta; x)/A_{\mathrm{coh}}(E, \vartheta; x)$, depends on x in a more complex way. However, it is simple to show that this dependence can be neglected. In fact, according to the definitions (7) and (10),

$$\frac{A_{\mathrm{inc}}(E', \vartheta; x)}{A_{\mathrm{coh}}(E, \vartheta; x)} \approx \frac{A_{\mathrm{coh}}(E', \vartheta; x)}{A_{\mathrm{coh}}(E, \vartheta; x)}. \tag{20}$$

At ϑ fixed and because A_{coh} is monotonic as a function of x (suppose that the greater density is ρ_2) we obtain

$$\frac{A_{\mathrm{coh}}(E; x)}{A_{\mathrm{coh}}(E; x)} \leqslant \frac{A_{\mathrm{coh}\ 2}(E')}{A_{\mathrm{coh}\ 1}(E)}, \tag{21}$$

whose maximum value, for a given stoichiometric composition of the sample, is easily obtained from the relation between E' and E (equation (5)).

In this way, the total scattered intensity I_{obs} at x is

$$I_{\mathrm{obs}}(x) = \chi I_0 PA(x)[n_1(x) I_1 + n_2(x) I_2], \tag{22}$$

where χ is a new constant, proportional to K in equation (15), which describes the dependence of K on the number of scattering centres.

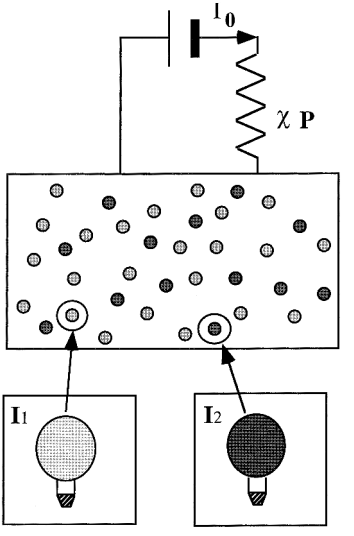

χ **P** Resistance of the electric circuit

$\mathbf{I_0}$ Current intensity

$\mathbf{n_1}$ Number of lamps of the first kind

$\mathbf{n_2}$ Number of lamps of the second kind

$\mathbf{I_k}$ Light intensity of a single lamp (k=1,2)

A Lamp glass opacity

Figure 7. Electric panel model of the EDXD method for phase transitions. (Reprinted with permission from [37]; copyright 1997 by Marcel Dekker, Inc.)

Equation (22) has a representation in terms of a very simple model, namely the 'electric panel model' [12]. It can help us to understand intuitively the basic meaning of the EDXD–PT technique that may be hidden by the previous symbols and calculation. Let us suppose that a certain number of two kinds of lamp having two different light intensities are mounted on an electric panel. A light detector is placed at a distance that is large compared with the dimensions of the panel. Now, leaving the total number of lamps unchanged, we replace some of the lamps of one kind with the same amount of lamps of the other kind. After this operation the intensity of light at the detector is measured. The essence of the EDXD–PT technique corresponds to the possibility of calculating the number of replaced lamps by just knowing the measured intensity. In this model all the quantities involved in equation (22) correspond to those relative to the panel model, as indicated in figure 7.

By substitution of the expressions for $n_1(x)$ and $n_2(x)$,

$$I_{\text{obs}}(x) = \chi I_0 PA(x)\left(\text{v}\frac{1-x}{(1-x)/\rho_1 + x/\rho_2}I_1 + \text{v}\frac{x}{(1-x)/\rho_1 + x/\rho_2}I_2\right). \tag{23}$$

The plausibility of this formula can be shown by writing the expression for the total observed intensity and considering the scattering matter as a whole (in the same way as for a sample consisting of only one component):

$$I_{\text{obs}}(x) = \chi I_0 PA(x)\, n(x) \langle I \rangle_x, \tag{24}$$

where $N(x) = \rho(x)\,\text{v}$ is the total number of scattering centres and $\langle I \rangle_x$ is the average intensity scattered by a single centre at x. Comparing the two equations, we have

$$\frac{1}{\rho(x)} = \frac{1-x}{\rho_1} + \frac{x}{\rho_2}, \quad \langle I \rangle_x = (1-x) I_1 + x I_2, \tag{25}$$

that is the sample density is simply the weighted harmonic average of the component densities and the mean scattered intensity is the same as for the constant-density case.

As for the constant-density case, measurements corresponding to $x = 0$ and $x = 1$ have to be utilized:

$$I_{\text{obs }1} = \chi \mathrm{v} I_0 P A_1 \rho_1 I_1,$$
$$I_{\text{obs }2} = \chi \mathrm{v} I_0 P A_2 \rho_2 I_2$$

and, by substitution,

$$I_{\text{obs}}(x) = A(x)\rho(x)\left(\frac{1-x}{A_1\rho_1} I_{\text{obs }1} + \frac{x}{A_2\rho_2} I_{\text{obs }2}\right). \tag{26}$$

Finally, defining

$$I_1^* = \frac{A(x)\rho(x)}{A_1\rho_1} I_{\text{obs }1}, \tag{27a}$$

$$I_2^* = \frac{A(x)\rho(x)}{A_2\rho_2} I_{\text{obs }2}, \tag{27b}$$

we obtain from equation (27) an expression quite similar to that for the constant-density case (equation (17)). It can be used to follow the time evolution of x by observing the changes in A and I_{obs} during the PT.

7.3. *Adaptation of the equation to the experimental apparatus*

The theoretical expression must be adapted in order for it to be used practically. From the experimental point of view, $A(x, \vartheta)$ and $\rho(x)$ in equations (27) can be calculated by X-ray absorption measurements at $\vartheta = 0$ as in section 4.2, equation (6):

$$\frac{\rho(x)}{\rho_i} = \frac{\ln[A(x, \vartheta = 0)]}{\ln[A_i(\vartheta = 0)]} \tag{28a}$$

$$\frac{A(x, \vartheta)}{A_i(\vartheta)} = \left(\frac{A(x, \vartheta = 0)}{A_i(\vartheta = 0)}\right)^{\sec \vartheta} \tag{28b}$$

where $i = 1, 2$.

Furthermore equation (26) must be modified to take into account the presence of a background produced by cell walls. Rewriting equation (12), we have

$$I_{\text{obs}}(x) = \chi \mathrm{v} I_0 P A^{\text{cell}} A(x)\rho(x) I(x) + A(x) I_{\text{emp}}, \tag{29}$$

where I_{emp} is the total scattered intensity by the cell walls. Both A^{cell} and I_{emp} do not depend on x. They can be measured once at the beginning of the measurement session and used to correct the remaining experimental data sets. Once $I(x) = I_{\text{obs}}(x) - A(x) I_{\text{emp}}$ and $I_i = I_{\text{obs}}(x) - A_i I_{\text{emp}}$, $i = 1, 2$, are defined, replacing $I_{\text{obs }1}$, $I_{\text{obs }2}$ and $I_{\text{obs}}(x)$ in equation (17) by I_1, I_2 and $I(x)$ respectively, another expression analytically similar to equations (26) and (16) is obtained; the presence of the cell does not disturb at all the measurements.

This utilization of EDXD in PTs is particularly convenient because, in this case, some of the advantages illustrated in section 2 are highly relevant, while the limitations have almost no effects. We can summarize the merits of this method in the following way.

(1) As the q interval is wider, there is a wider choice of the zone where the diffraction patterns of the two phases can be compared. In equation (16), the larger the difference between the diffracted intensities I_1 and I_2, the more precisely the value of x is determined.

(2) The reduction in the acquisition time enables one, at a parity of statistical uncertainty, to study more rapid transitions.
(3) The kinetics as a function of a free parameter, such as the temperature or pressure, can be easily studied.
(4) If the measured system undergoes a change during data collection, in ADXD the various points of the spectrum correspond to different stages of the process: the first indicates the initial phase, the central to an intermediate phase and the last to the final phase. In EDXD all the points contain the same information being collected simultaneously and there are no inhomogeneities in the various regions of each spectrum.
(5) The comparison between the diffraction spectra necessary to obtain the transition coordinates can be executed directly using the observed profiles with no need for deconvolution.
(6) The problem from the correction of the raw data is almost completely bypassed because, since x is obtained by the ratio between the differences of the spectra (equation (17)), both the additive and the multiplicative contributions to the observed intensity that do not change during the transition are automatically eliminated. In [10, 12] it has been demonstrated that, at least to a very good approximation, the totality of the effects that accompany single elastic scattering (and that do not give information about the transition kinetics), produce just additive or multiplicative terms in the observed intensity.
(7) Unlike the ordinary EDXD measurements that are carried out to obtain the structure factor, in the EDXD applied to PTs the combination of diffraction spectra corresponding to various q ranges is not required. The collection of just one spectrum is sufficient to obtain the evolution of x.

In the context of the merits of the EDXD–PT technique, we can discuss also the advantage that it has with respect to the other techniques usually utilized to follow the evolution of a system undergoing a phase transition, such as differential scanning calorimetry (DSC) and infrared vibrational spectroscopy [11]. In comparison with these, the EDXD–PT method has a fundamental advantage, for these techniques are based on the observation of an effect somehow connected to the change in the sample structure and not on the observation of the change itself. DSC is based on the detection of the heat (enthalpy) flux produced or absorbed by the sample during the PT (the latent heat of transition). During the transition the temperature is constant; therefore the enthalpy exchange is directly proportional to the change in the configurational entropy. If the entropies of the initial and final phases of the system are almost the same, no flux will be detected. Instead the EDXD–PT method is able to reveal a change in the structure even if it does not involve a variation in the entropy, because it is sensitive to the modification of the microscopic arrangements of the system, even if the two phases are characterized by the same degree of disorder. In fact, two different arrangements will produce different modulations in the scattered X-ray beam, regardless of whether they have the same entropy or not.

Moreover, DSC gives just an overall indication of the transition that is occurring because the exchanged heat can be due to the modification of any of the structures contained in the sample (consider for instance polymers) and on any scale (short-, medium- or long-range rearrangements). In contrast, the EDXD–PT technique can distinguish the range of the distances at which the modifications occur; changing the

angle of scattering, it is possible 'to frame' different regions of the reciprocal space and, therefore, different ranges of distances.

On the other hand, infrared spectroscopy is useful just when, owing to the PT, some new peaks appear or old peaks disappear in the vibrational spectrum, that is if some degrees of freedom are blocked or activated by the transformation. However, such a change in the spectrum may or may not happen and the result of this method is uncertain. The optical methods sometimes used are subject to similar limitations, being connected to possible but not necessary variations in the refraction index of the sample.

8. Diffraction experiments

EDXD can be used in several types of investigation including structural studies as well as kinetic studies. Liquids [13–22], amorphous samples and powders with a low degree of crystallinity [23–33] can be characterized by this technique. Furthermore, *in-situ* PTs were also studied [11, 12, 34–39]. In the forthcoming sections a few examples of the possible applications will be shown, although for more details a full bibliography is given in the references section.

8.1. *Kinetic studies: experiment*

The aim of the EDXD–PT measurements is to collect a sequence of diffraction spectra while a system undergoing a PT is changing. The scheme of the cell used for this purpose is presented in figure 8. The spectra represent 'snapshots' of the system taken in the reciprocal space during its evolution from the initial to the final structure, a time-resolved imaging of its reciprocal lattice. In order to obtain the evolution parameter $x(t)$, each spectrum must be weighted by a coefficient connected to the density of the sample at the moment at which the diffraction spectrum is taken, according to equations (26) and (27). To calculate these coefficients a series of transmission spectra (i.e. $\vartheta = 0$) must also be collected with the same modalities as the diffraction spectra. This means that the sample must be put twice in the initial condition and twice irradiated by two series of X-ray flashes. The first series is taken with the diffractometer arms forming an angle 2ϑ (diffraction measurements), and the second series with the diffractometer arms aligned (transmission measurements). The time scan of the two series must be the same, so that each diffraction spectrum will correspond to the transmission spectrum collected at the same stage of the transformation.

From the practical point of view, it is worth doing a preliminary diffraction measurement of the sample to fix the scattering angle ϑ. The best experimental conditions are met when some of the diffraction peaks that will shift or disappear during the transition are contained in the q range scanned at ϑ. In this way, the difference between the initial and final spectra will be greater and, consequently, there will be a proportional reduction in the statistical noise. However, it does not mean that the method is suitable only when diffraction peaks are present. Various experiments showed that, because of the redundant information contained in the spectra, $x(t)$ can be obtained even when the transition is between two disordered structures that do not produce any well defined peak (so that the initial and final spectra cannot be distinguished by the naked eye).

Another empirical prescription is to choose low values of ϑ. In this condition, the value of I_{inc} (equation (15)) is small (because it vanishes when ϑ approaches zero) while the coherent contribution is a maximum [3]. Since the determination of x is based on the change in the latter, while the former produces just statistical noise which is almost

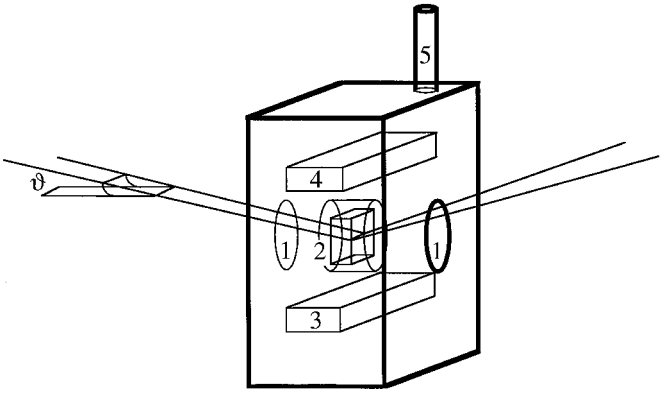

Figure 8. Schematic design of the variable-temperature cell: 1, Mylar windows; 2, sample holder; 3, heat source (electric heater); 4, cold source (frozen liquids or liquid-nitrogen container); 5, vacuum pipe. (Reprinted with permission from [37]; copyright 1997 by Marcel Dekker, Inc.)

constant during the transition, a small angle should be preferred. Furthermore, at small angles, the approximation in equation (20) is fulfilled better because the Compton shift (equation (5)) is an increasing function of sin ϑ.

In the previous section we illustrated the application of EDXD to the study of systems that change their structural properties as a function of time. Some of those materials have a technological interest and it is very important in those cases to determine which structural changes occur and in which time scale. A great deal of work has been done lately on polymer PTs.

8.2. *Polymer phase transitions*

A new generation of non-conventional batteries in recent production is based on the conductive properties of polymers, because of the favoured ionic motion of salts doping the polymeric matrix [40–45]. However, transport is possible only if the chains are flexible enough, that is above the melting temperature T_m (in a liquid) or in an amorphous phase above the glass transition temperature T_g. In the glassy or crystalline phase the macromolecules are rigid and become a barrier to ion transport. Two ways are usually employed to slow the transition of liquid or amorphous polymers to crystalline polymers: by keeping the battery at a suitable temperature or by doping the polymer to slow the spontaneous tendency to the crystallization [37].

Therefore, it is extremely important to determine the transition kinetics of these conducting polymers (from amorphous to crystalline and vice versa). In this section, the results of three investigations on poly(ethylene oxide) (PEO) PTs studied by EDXD will be presented. When PEO is melted and rapidly quenched at a temperature T between T_m and T_g, it retains for some time its initial amorphous structure. However, PEO is not stable in this condition and will undergo a transition to a crystalline structure.

The application of the EDXD technique in this case enables the dynamics of this phase to be followed. In particular it is possible to determine the stage of the transition directly, completely bypassing the extraction of the structure factor, as was shown in sections 7.1 and 7.2. In this way all the uncertainties due to the use of theoretical values or descriptive models of the quantities involved in the scattering process are avoided. The PTs of PEO are a check of the reliability of the method.

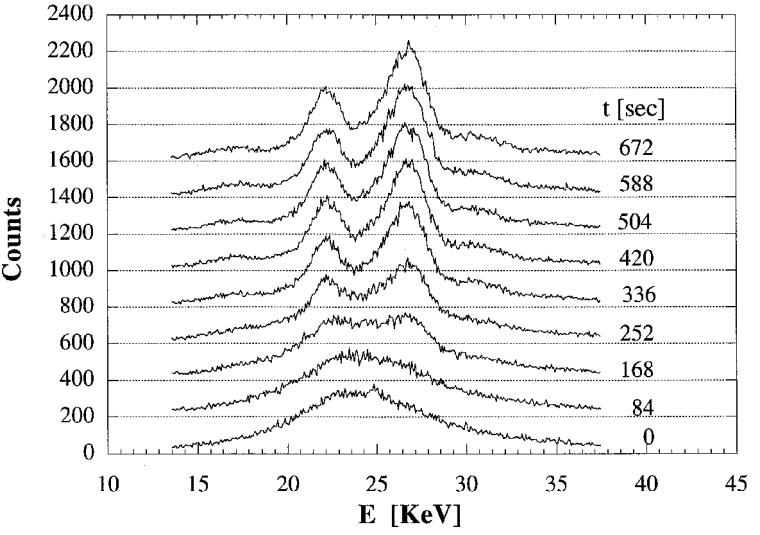

Figure 9. A sampling of the diffraction spectra at $\theta = 3.5^{\circ}$. Each spectrum has been shifted along the axis of ordinates by 200 units with respect to the previous spectrum. (Reprinted with permission from [11]; copyright 1996 by Marcel Dekker, Inc.)

A preliminary set of measurements on crystalline PEO was performed to find the angular position corresponding to the maximum scattered intensity. This is particularly important, since the transition period is short, and it is essential to maximize the signal-to-noise ratio. Among all the peaks that can be used, those placed at the lowest q values are chosen to minimize the effects of the incoherent contribution to the total intensity.

The measurements are performed by irradiation of the sample with X-ray flashes. The diffraction spectra are collected and automatically stored every Δt_1 s. The duration of each flash is Δt_2. In practice a continuous acquisition was divided into intervals of 28 s (Δt_2) separated only by negligible pauses to store the spectra (Δt_1 about zero). In figure 9, every third spectrum is reported.

In the same way after a new heat treatment, transmission measurements at $\vartheta = 0$ are accomplished with the same time sampling. They are used to calculate the density changes on passing from the amorphous to the crystalline state.

In the analysis, the low- and high-energy range channels are neglected, the former because the Lambert–Beer law (section 4.2) breaks down, and the latter because the intensity of the incident beam is too low and also because the X-rays become more penetrating, making the sample almost transparent in both phases.

Finally the plot of the transformation coordinate is obtained as a function of time (according to equation (17)). The statistical distribution of one of these points is shown in figure 10. The points can be fitted by a Liquori–Tripiciano curve $x(t) = [1 - \exp(-t/\tau_1)]/[1 - \exp(-t/\tau_1) + \exp(-t/\tau_2)]$ for phase transitions (figure 11), with satisfactory agreement. The statistical information can be used to attribute a level of confidence to the experimental points (error bars in figure 11).

Once it was established that EDXD enables one to follow the PTs, various crystallization processes of PEO were studied. The experiment differs in the temperature of quenching of the sample. In order to obtain a 'standard' liquid polymer, PEO was heated at 100 °C for 1 h to avoid spontaneous nucleation from pre-

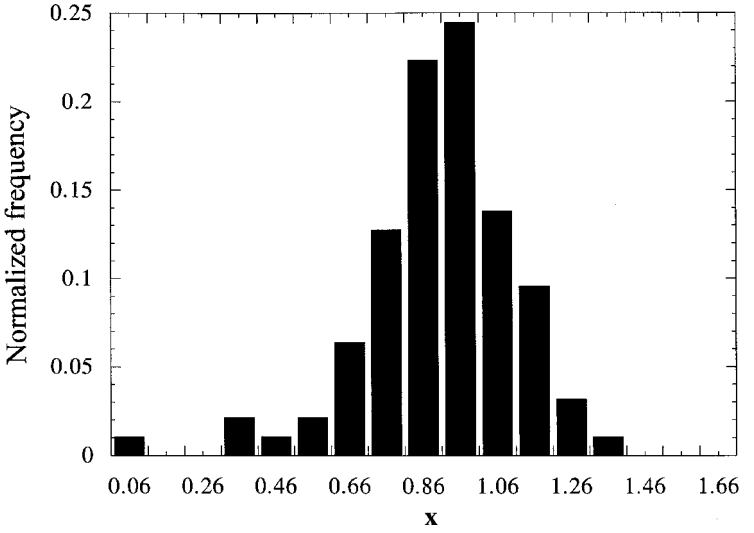

Figure 10. Normalized distribution of x (t_{15} = 392 s). (Reprinted with permission from [11]; copyright 1996 by Marcel Dekker, Inc.)

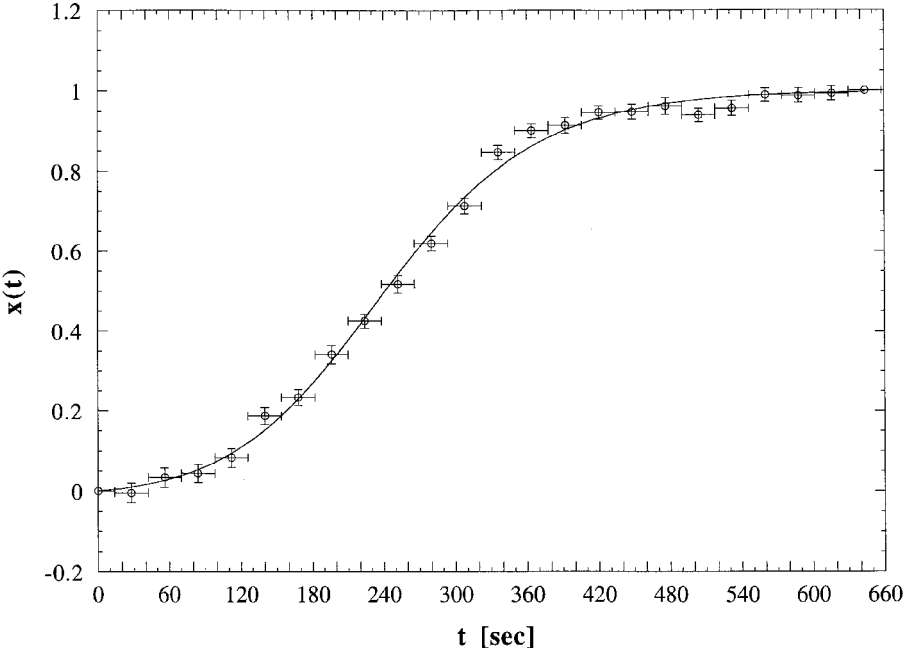

Figure 11. Plot of the transformation coordinate $x(t)$, where the abscissa and ordinate error bars are analogous to those of figure 10: (——), the Liquori–Tripiciano law fit. τ_1 = 3921.8± 495.1 s and τ_2 = 85.6± 3.4 s are its phenomenological parameter values. (Reprinted with permission from [11]; copyright 1996 by Marcel Dekker, Inc.)

existing microcrystals that may be not completely dissolved during melting. Then it was rapidly cooled to the final temperature T in a time short compared with the characteristic time of crystallization.

Another set of measurements was then made to observe the opposite process of melting. In this case a crystalline was quickly heated at a temperature above T_m. Since

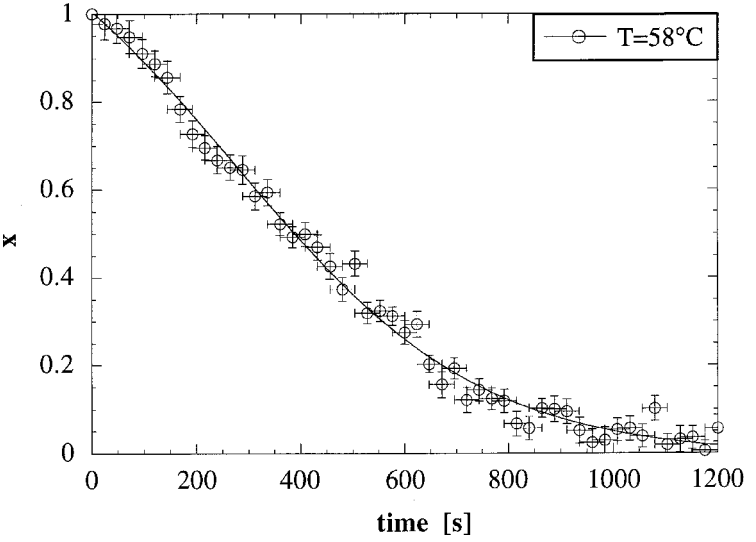

Figure 12. Plot of x against t at $T = 58$ °C during melting, together with its sigmoidal fit. The horizontal error bars represent the acquisition time; the vertical error bars are the standard deviation of the x distribution. (Reprinted with permission from [12]; copyright 1997 by Marcel Dekker, Inc.)

the thermal history of a crystalline polymer influences its texture and this, in turn, might produce differences in the experiments, a standard crystalline polymer was made each time by cooling the molten polymer to 50 °C. The equilibration at the working temperature is also very critical because at some temperatures the transformation can be very fast. After the transformation is concluded, the sample is converted again into the initial state and the transmission measurements are performed as illustrated in section 8.1.

The time evolution of x (equation (26); section 7.2) was investigated in a range of T between 45 °C and T_m for crystallization and between T_m and 81 °C for melting. From the point of view of the transition kinetics, T_m represents the temperature at which the transition speed approaches zero, that is the highest temperature at which the crystalline polymer remains indefinitely in the initial phase as well as the lowest temperature at which the liquid remains indefinitely amorphous. After the initial thermal cycles, T_m was found to be 56 °C. In figure 12 the transition coordinate corresponding to the temperature 58 °C is plotted as a function of time.

The transition speed can be calculated either by considering the instant t^* at which half of the mass of the sample is converted, or by calculating the slope of the tangent at the inflection point, that is the maximum transition rate. However, it is difficult to determine which is the first spectrum collected after equilibration of the sample so that it is not possible to establish which is the first experimental point; the initial state must be the state at which, although the system is still liquid, its temperature is T. As a consequence, it is more reliable to calculate the speed through the slope of the tangent. Therefore, the set of experimental points was fitted with a sigmoidal curve that was then derived to obtain the maximum transition rate v_{max}. In figures 13 (a) and (b) some of the plots of x against t for crystallization and melting respectively are shown. The maximum v_{max} of the time derivative of the preceding curves can be plotted to represent the behaviour of the kinetic as a function of the temperature T (figure 14).

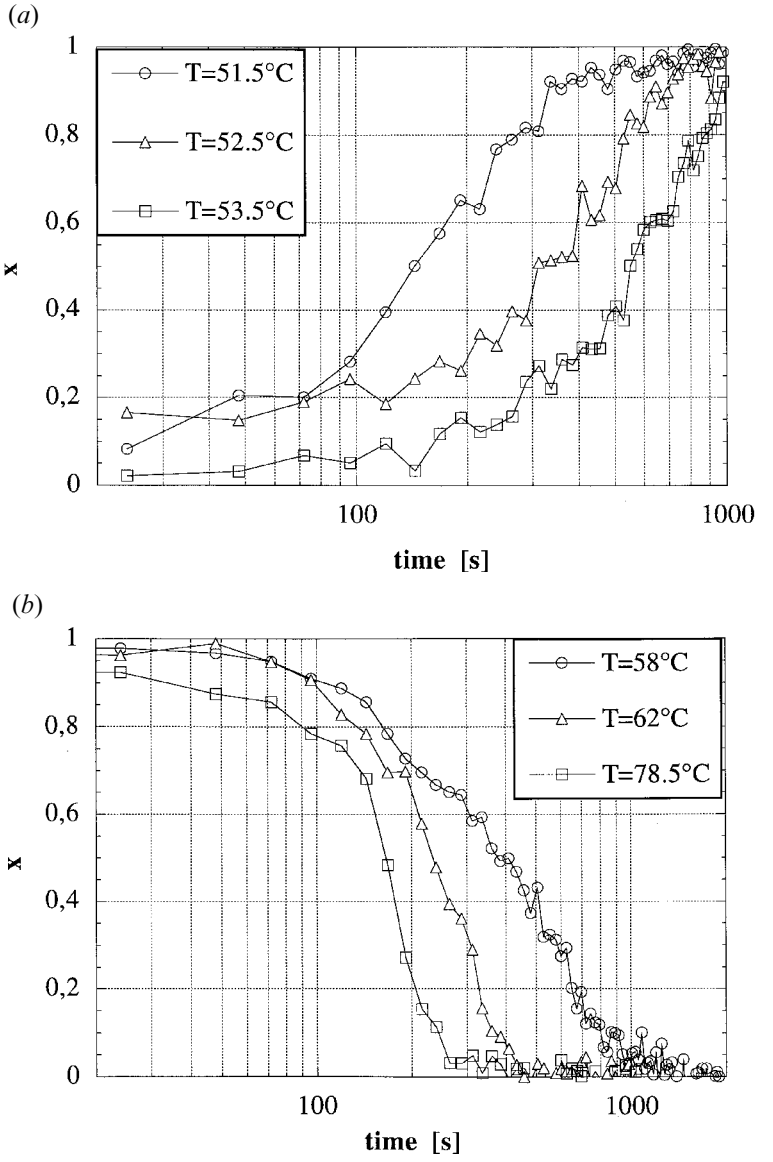

Figure 13. Semilogarithmic plots of x against t at various temperatures for (*a*) the crystallization and (*b*) the melting processes. The error bars are not drawn as the graph would appear too confused. The x profiles are quite similar in the two cases regardless of the different transformation mechanisms. (Reprinted with permission from [12]; copyright 1997 by Marcel Dekker, Inc.)

The points below T_m reproduce the right-hand part of the well known bell-shaped curve of the polymer crystallization rate. They do not provide original information and can be considered just a confirmation of the correctness of the method. Instead, points above T_m show an interesting behaviour never observed before. They can be divided into two sets: one in the range $T_m < T < T^*$ and the other for $T > T^*$, with $T^* = 76\ ^\circ C$. In the lower-temperature zone, v_{max} is a convex increasing function of temperature while, in the upper zone, the slope increases abruptly.

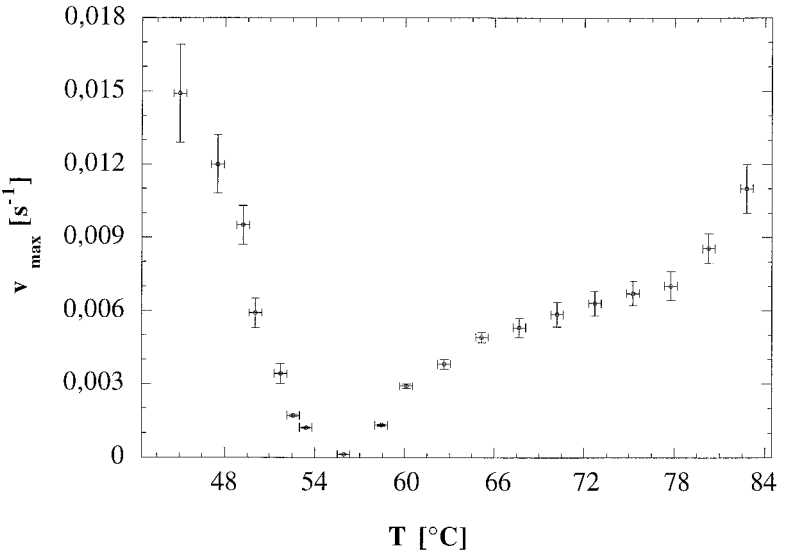

Figure 14. Absolute value of v_{max} as a function of T. In a graph such as this the melting temperature T_m is the abscissa of the point with the ordinate $v_{max} = 0$. Therefore it must be close to the temperature of the point with the lowest v_{max}, that is $T_m \approx 56$ °C. If $T > T_m$, the points represent transitions from the crystalline to the amorphous phase; if $T < T_m$, they represent the inverse transitions. As T moves away from T_m, the vertical error bars become progressively wider, showing the limit of the present technique. (Reprinted with permission from [12]; copyright 1997 by Marcel Dekker, Inc.)

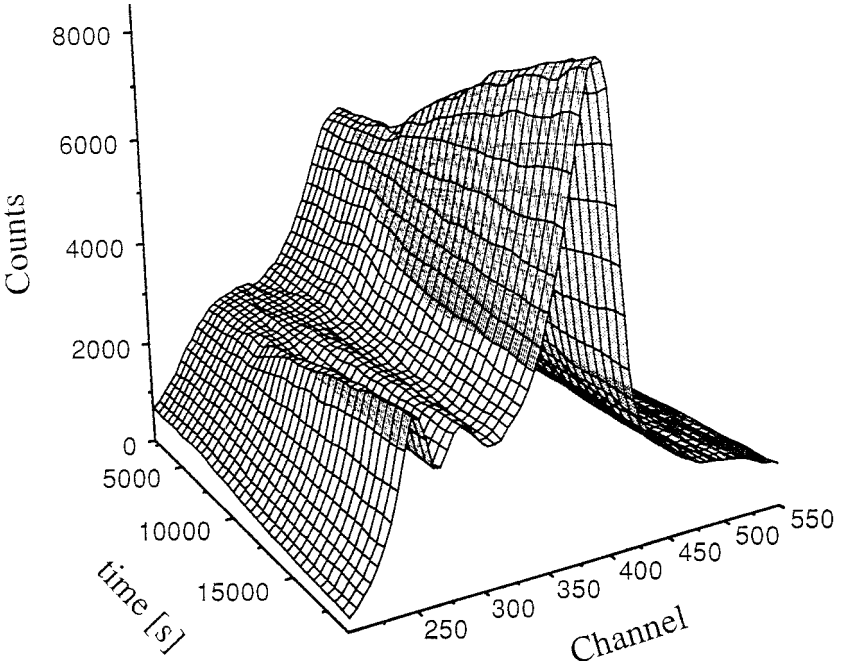

Figure 15. Three-dimensional plot of diffraction spectra collected at various times of the $[PEO]_8$–$[LiClO_4]$ solution. On the vertical axis the channel index j is reported, the energy being linearly dependent on it according to the following relation: $E = (0.0614j + 0.052)$ keV. (Reprinted with permission from [37]; copyright 1997 by Marcel Dekker, Inc.)

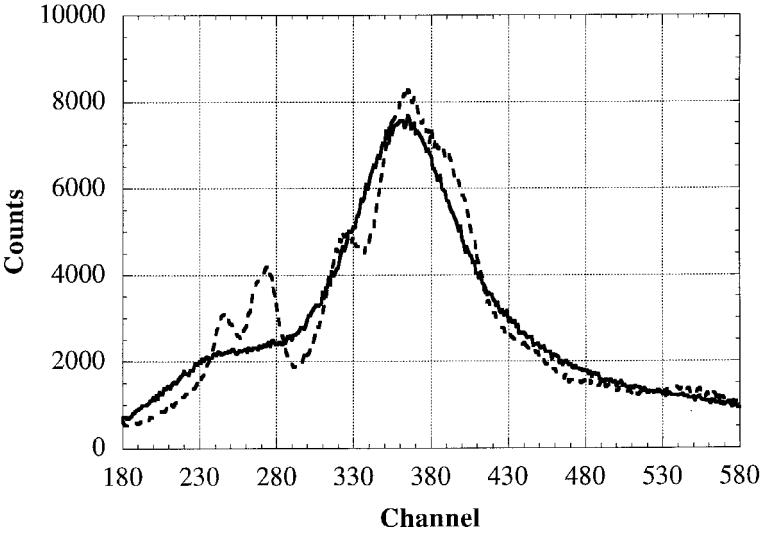

Figure 16. The same comparison in the case of $[PEO]_8$–$[NaClO_4]$ solution at the beginning (——) and at the end (– – – –) of the phase transition. (Reprinted with permission from [37]; copyright 1997 by Marcel Dekker, Inc.)

Although the two processes of crystallization and melting are not equivalent, they show a similar evolution of the transition coordinate x. In both cases it is possible to fit x with a sigmoidal curve and, if x is defined as the fraction of the sample in the final state (regardless of whether it is a crystal or a liquid), it would be impossible to establish which process the graph represents by just looking at it. This implies similar transition mechanisms in both the crystallization and the melting processes.

Crystallization is activated by small particles present in the liquid. They may be impurities or crystalline domains that either survived during heating or were formed by spontaneous organization of polymer chains. On these particles, other chains can sediment, increasing the surface available for further sedimentation.

Therefore, a mechanism similar to this nucleation must be present also in the melting process. The mechanism is probably the creation of free volume, due to heating of the sample. This produces vacancies in the bulk that can receive the polymers that leave the surface of crystal domains; the expansion would allow a reduction in the packing and, as a consequence, in the hydrostatic pressure exerted on the polymer chains. The resulting increase in the mobility would cause the beginning of the melting.

In all the measurements the initial part of the plot of x against t is very short and the system begins almost immediately to transform itself into the final state. Once the transition has started, x always rises with a rate that increases in absolute value until $x^* \approx 0.5$. Above this value it decreases and finally approaches an asymptotic value of unity.

An example of the effect of salts on the polymer structure (and as a consequence on the conductivity) is given by a study of the PEO PT upon doping with different concentrations of alkaline salts [37]. A kinetic study of the PT was performed on PEO with different salts and at different concentrations, quenching the liquid sample to room temperature. The doping alkaline elements were lithium, sodium and potassium

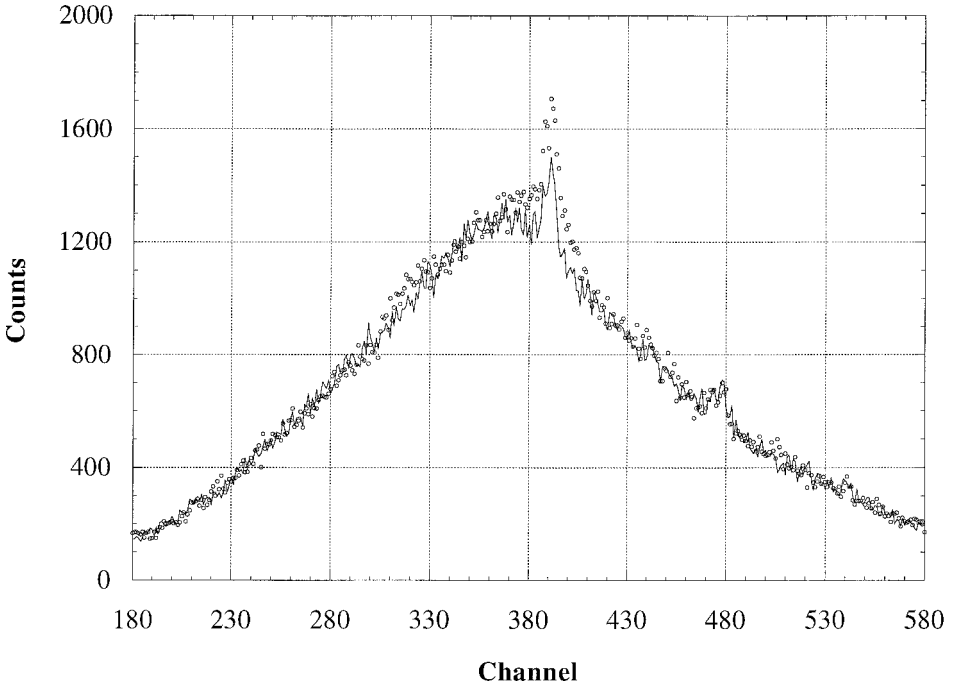

Figure 17. Comparison between the initial (——) and the final (·) spectra in the crystallization of the $[PEO]_{12}$–$[LiClO_4]$ compound. The structures appear to be very similar and only the use of a statistical procedure makes it possible to detect the evolution of the system. (Reprinted with permission from [37]; copyright 1997 by Marcel Dekker, Inc.)

with the ratios of alkaline element to PEO of 1:12 or 1:8 (except for potassium, which has been prepared only in the ratio 1:12).

The solutions were prepared by heating a mixture of the polymer and salt in suitable proportions. The supposed structure PEO–alkaline ion entails coordination through the oxygen atoms, with the polymer chains wrapped around the cations so that the latter are trapped inside. The transition kinetics have been followed as described above. In figure 15 (*a*) a sequence of diffraction spectra, corresponding to the $LiClO_4$–PEO 1:8 solution are shown as a function of energy and of time.

The presence of alkaline cation affects not only the crystallization rate, which is much slower, but also the final structure, which is less ordered than pure PEO. However, this is evident only for higher-concentration samples as a comparison of figures 16 and 17 shows. The transition coordinates as a function of time have been fitted with Liquori–Tripiciano curves and v_{max} was calculated as before for pure PEO.

The results of the measurements show that, at a ratio of salt to polymer of 1:12, the presence of a different alkaline cation does not affect the crystallization speed. This means that the concentration of alkaline cations is too low to influence the speed at which the polymer tends to arrange in ordered structures (figure 18). Above a certain threshold, ranging from 1:12 to 1:8, the dimension of the cations begins to play a role.

Measurements of the solution $[PEO]_8$–$[LiClO_4]$, which is more interesting from a technological point of view, as the charge transfer is proportional to the number of available carriers, are simpler and more reliable. The characteristic crystalline feature

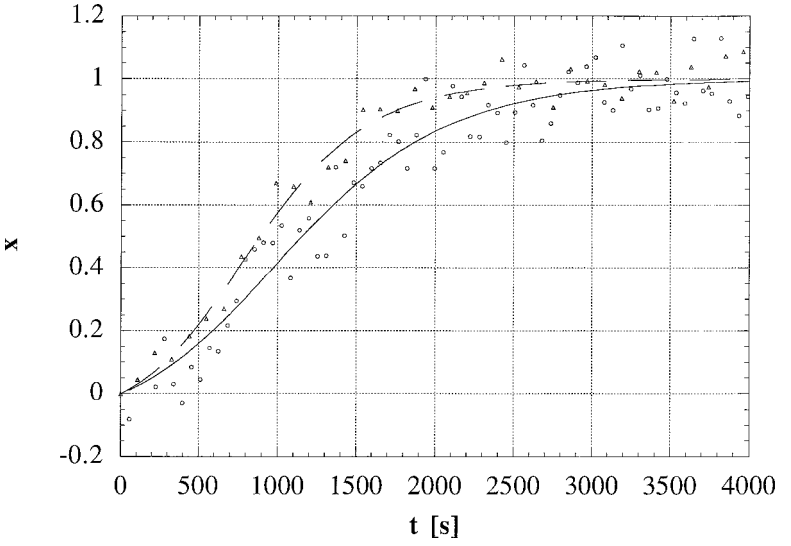

Figure 18. Plot of the transition coordinate as a function of time for the $[PEO]_{12}$–$[XClO_4]$ solution: (△), X = Li; (○), X = Na; (——), the Liquori–Tripiciano fit. The scattering of the experimental data is produced by the uncertainty due to the resemblance between the initial and final structures (see figure 17). In fact, when there are small differences between I_1, I_2 and $I(x)$, the statistical noise of x becomes very high (equation (17)). (Reprinted with permission from [37]; copyright 1997 by Marcel Dekker, Inc.)

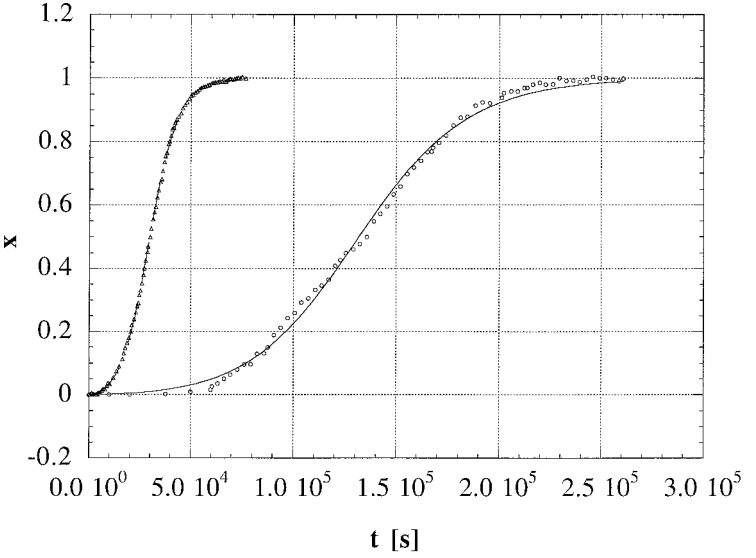

Figure 19. Plot as in figure 18 for the same $[PEO]_8/[XClO_4]$ compounds with a higher concentration of cations: (△), X = Li; (○), X = Na. (Reprinted with permission from [37]; copyright 1997 by Marcel Dekker, Inc.)

clearly appears in the spectrum and it allows a more precise determination of the transition coordinate. Furthermore the crystallization rate is lower so that the spectra can be collected for a longer time, and hence with better statistics (figure 19). For these reasons the effect is measured with high confidence. Moreover, the slowing down of

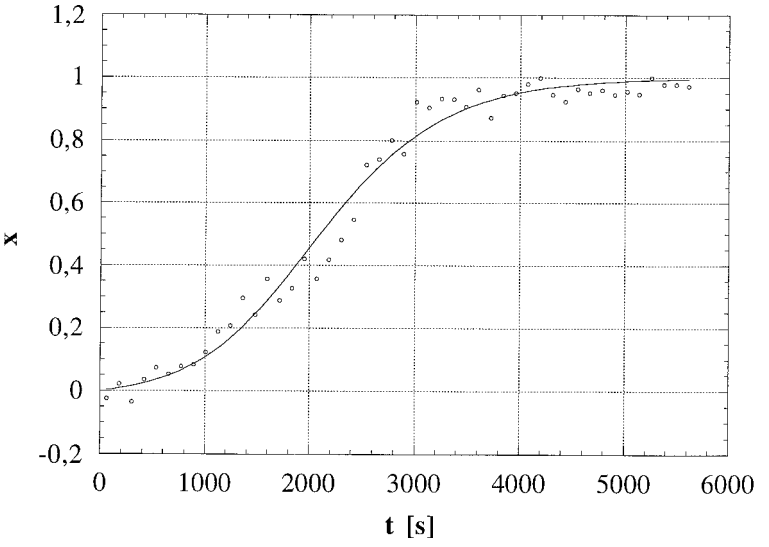

Figure 20. Graph analogous to figure 19 for the $[PEO]_{12}$–$[KClO_4]$ compounds. (Reprinted with permission from [37]; copyright 1997 by Marcel Dekker, Inc.)

the kinetics allows good equilibration of the sample to the measurement temperature. In this condition, possible thermal gradients inside the system will disappear in a time that is negligible with respect to the characteristic transition time, providing the best working conditions.

The main effect is the decrease in the crystallization rate due to the increased concentration of salts. For the lithium-doped sample, v_{max} is more than one order of magnitude, while the effect of sodium doping is even larger (almost two orders of magnitude). These behaviours are consistent with the hypothesis that the affinity between PEO oxygen atoms and doping cations induce crystallisation in lamellae with the cations wrapped inside the polymer spirals. The cation concentration in the polymeric solution is a very critical parameter. The cation capability to bind different polymeric chains while hindering the chain motions to find a stable configuration favours the formation of cation–polymer chain couples which inhibits the ionic transport. The effects of lithium and sodium at higher concentrations are quite different, since the larger size of sodium is more effective in preventing an ordered arrangement of polymer chains. Finally the time evolution of x for $KClO_4$ is plotted in figure 20 only for the lower concentration (1:12). The crystallization time for the 1:8 compound was too long to be observed in a measurement session of reasonable duration.

As we have already stated concerning the model to justify the observed behaviour during crystallization, the latter takes place when, in a liquid polymer quenched below T_m the free flexible chains find solid nuclei on which they can sediment. These nuclei play the role of catalysts in the process and the time of crystallization depends dramatically on their number and dimensions. Hence, although in ideal conditions the crystallization of a liquid polymer (after quenching to a temperature T_c below T_m) should not depend on T nor on the time of permanence at T, yet both these parameters influence it. In particular, the crystallization time is found to become longer, the higher T, and the longer that the polymer remains at T. This effect is attributed to the

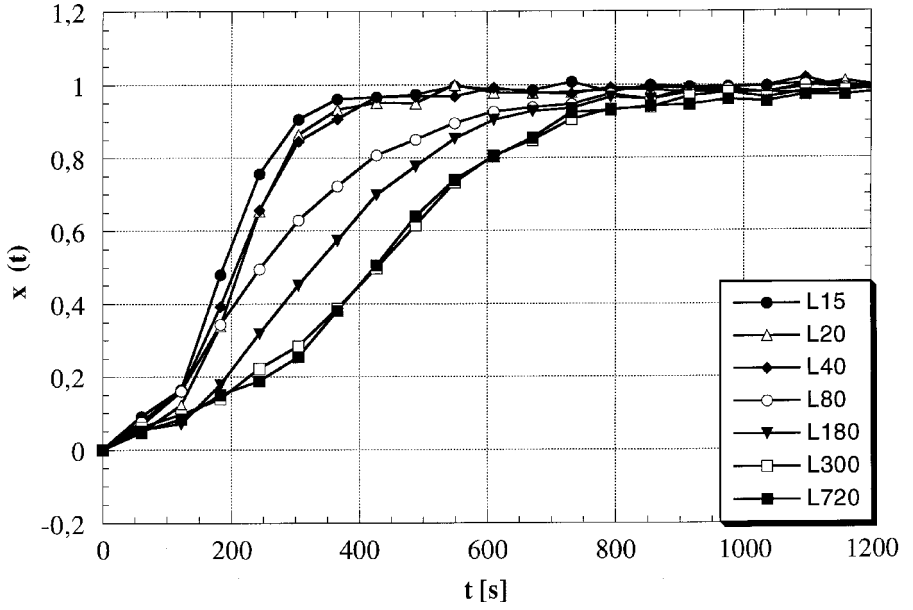

Figure 21. The family of transition curves for various times t^* of residence at a temperature $T(1) = 112\,^{\circ}C$; from left to right, $t^* = 15$, 20, 40, 80, 180, 300 and 720 min. (Reprinted with permission from [38]; copyright 1999 by Marcel Dekker, Inc.)

incomplete dissolution of the crystalline domain during the residence of the polymer at T [46, 47].

To check the importance of this effect, we used a sample of poly(ethylene succinate) (PES), (Aldrich 18,203-6) having the following stoichiometric formula $(OCH_2{-}CH_2O_2{-}CCH_2{-}CH_2{-}CO)_n$ [38]. The sample, initially crystalline, was held at a fixed temperature $T(1) = 112\,^{\circ}C$ for a given residence time t^* and then quenched to the crystallization temperature $T_c = 80\,^{\circ}C$, with a cooling rate of $200\,^{\circ}C\ min^{-1}$. As usual, diffraction spectra were taken during the crystallization process.

After this, the sample was reset, by a suitable thermal treatment, to the initial crystalline state and the procedure was repeated many times, leaving all the conditions except t^* unchanged. In this way the effect of t^* on the crystallization kinetics was observed. In figure 21 the $x(t)$ curves corresponding to various choices of t^* (15, 20, 40, 80, 180, 300 and 720 min) are plotted. In figure 22 the maximum crystallization rates are shown together with the theoretical fit according to Alfonso's model. In figure 23 a graph analogous to figure 23, but for $T(2) = 116\,^{\circ}C$, is reported.

8.3. *Crystallization of an amorphous alloy: $Ni_{40}B_{60}$*

The study of crystallization of amorphous alloys is essential for the understanding of their physical and technological properties [48–51]. The crystallization of a phase whose composition is different from that of the amorphous phase is commonly called primary crystallization and is typical of the first step of crystallization of many amorphous metal–metalloid alloys [48, 49]. The primary crystallization stops when metastable equilibrium between primary crystals and the residual amorphous phase is reached. Subsequently the crystallization of the residual matrix can start (in some cases just at higher temperatures) [48, 49].

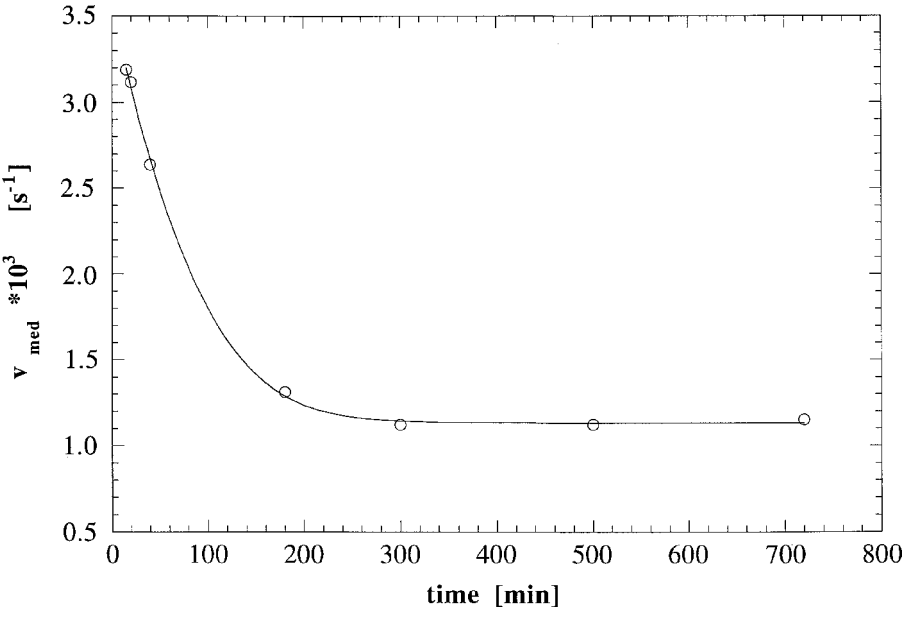

Figure 22. Plot of the crystallization rate obtained from the curves showed in figure 21, fitted by the theoretical Liquori–Tripiciano model $T = T(1) = 112\ ^{\circ}C$. (Reprinted with permission from [38]; copyright 1999 by Marcel Dekker, Inc.)

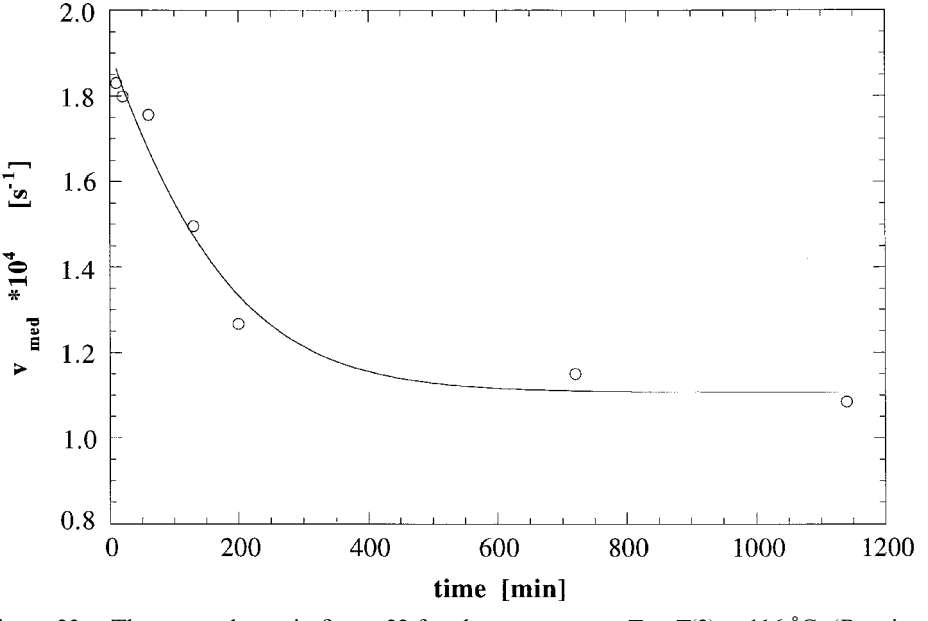

Figure 23. The same plot as in figure 22 for the temperature $T = T(2) = 116\ ^{\circ}C$. (Reprinted with permission from [38]; copyright 1999 by Marcel Dekker, Inc.)

An application of EDXD to this field is the study of crystallization of $Ni_{60}B_{40}$ amorphous alloy. The sample changes from an amorphous to a crystalline state as can be seen in figure 24 where the first spectrum (on the left) and the last (on the right) are reported. The spectra as functions of time show the growth of a crystalline phase which

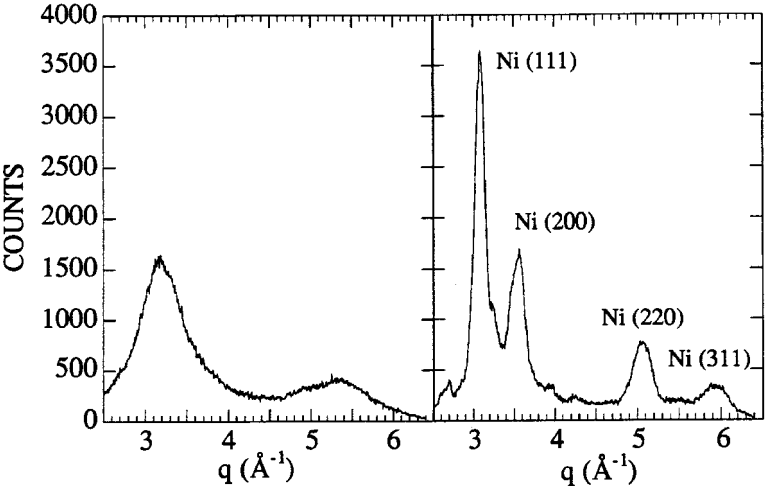

Figure 24. Diffraction spectra of the as-prepared (left) and crystallized (right) samples, corresponding to the first spectrum and to the last spectrum respectively. (Reprinted with permission from [36]; copyright 1997 by Società Chimica Italiana.)

can be identified as fcc nickel, through the appearance of four peaks with indices (111), (200), (220) and (311). The presence of a small amount of a second crystalline phase, orthorhombic Ni_3B, was also revealed. In our case, we interpret the results of the experiment in terms of a complete primary crystallization of fcc nickel.

Here the kinetics of isothermal crystallisation processes are described by the Johnson–Mehl–Avrami transformation equation

$$x(t) = 1 - \exp(-bt^n), \tag{30}$$

where $x(t)$ is the volume crystallized after a time t, and b and n are constants. To reproduce the Avrami curve we consider the intermediate spectra as a linear combination of the two extreme spectra:

$$I_i(q) = x_i I_{51}(q) + (1 - x_i) I_1(q). \tag{31}$$

This way we obtain an Avrami (figure 25) coefficient $n = 1.8$, close to the value predicted by the theory ($n = 1.5$) when primary crystallization due to the growth of quenched-in nuclei occurs.

The EDXD technique can be applied to the determination of structural long-range changes in materials. Studies have been performed on a silico-aluminate, cancrinite, of mineralogical interest.

8.4. *Cancrinite*

Cancrinite is a silico-aluminate with an ordered distribution of silicon and aluminium inside the tetrahedron constituting the framework [52–56]. The AB-type stacking sequence gives rise to two cages and a large channel for every unit cell. The cancrinite cages contain $[NaH_2O]$ clusters, while the large channels house the remaining cations (Na^+ and Ca^+) and anions (CO_3^-, SO_4^-, F^- and Cl^-). This mineral can be found in a large number of superstructures depending on the ordering of the vacancies inside the channels. The existence of various structures is due to the non-

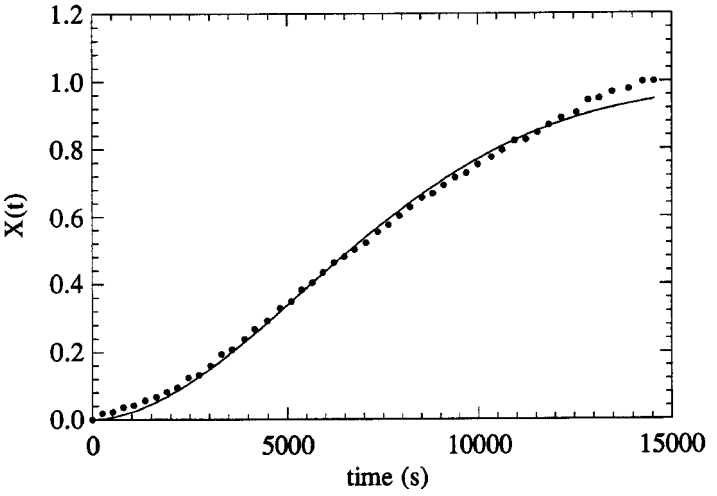

Figure 25. The Johnson–Mehl–Avrami equation nonlinear fit (——) of the crystallized volume fraction $x(t)$ (·). (Reprinted with permission from [36]; copyright 1997 by Società Chimica Italiana.)

stoichiometry of the solid. The thermal effects on such a material can be large, because of the possibility of water release from the cages. Ballirano *et al.* [35] studied the cancrinite structure as a function of temperature by EDXD and Fourier transform infrared spectroscopy. In particular, the heating process was carried out by increasing the temperature stepwise from 24 to 600 °C. Spectra were recorded at 24, 105, 206, 300, 403, 453, 500, 550, 569.5, 592.5 and 600 °C (figure 26). As a function of the temperature the cancrinite structure displays some changes, since the peaks in the X-ray diffraction patterns show shifts, broadening and intensity changes. The analysis of the changes in the diffraction pattern after cooling the sample shows a variation in the cell parameters of −0.1% (*a* parameter) and −0.3% (*c* parameter). It is hypothesized that the structure changes are due to a displacement of sodium atoms inside the cancrinite cage with respect to the original material. Furthermore, a water loss occurs, yielding an anhydrous phase that does not show any tendency to re-acquire molecular water.

8.5. *Interaction between* 1,4-*dihydropyridines and biological membranes*

One of the latest applications of the EDXD technique to kinetic studies involves the interaction between 1,4-dihydropyridine (DHP) and biological membranes [39]. These DHPs are a class of amphiphylic molecules that inhibit opening of voltage-dependent calcium channels and are used as antihypertensive agents for the treatment of angina and many other vascular diseases [57–61]. The study of the structural effects of these molecules on the membranes provides information about the role played by these changes in the regulation of ionic transport properties.

The interaction of two DHPs, nifedipine and lacidipine, with a model membrane has been studied. The study of lacipidine interacting with membranes is important since it persistently inhibits the voltage-dependent calcium channel. Moreover there is an evidence of a large partition coefficient in the hydrocarbon phase. It suggests that the excess of lacipidine remains in equilibrium with the membrane bilayer for times much longer than that for recording patch-clamp experiments.

The EDXD technique has been applied first to study the variation in an ordered

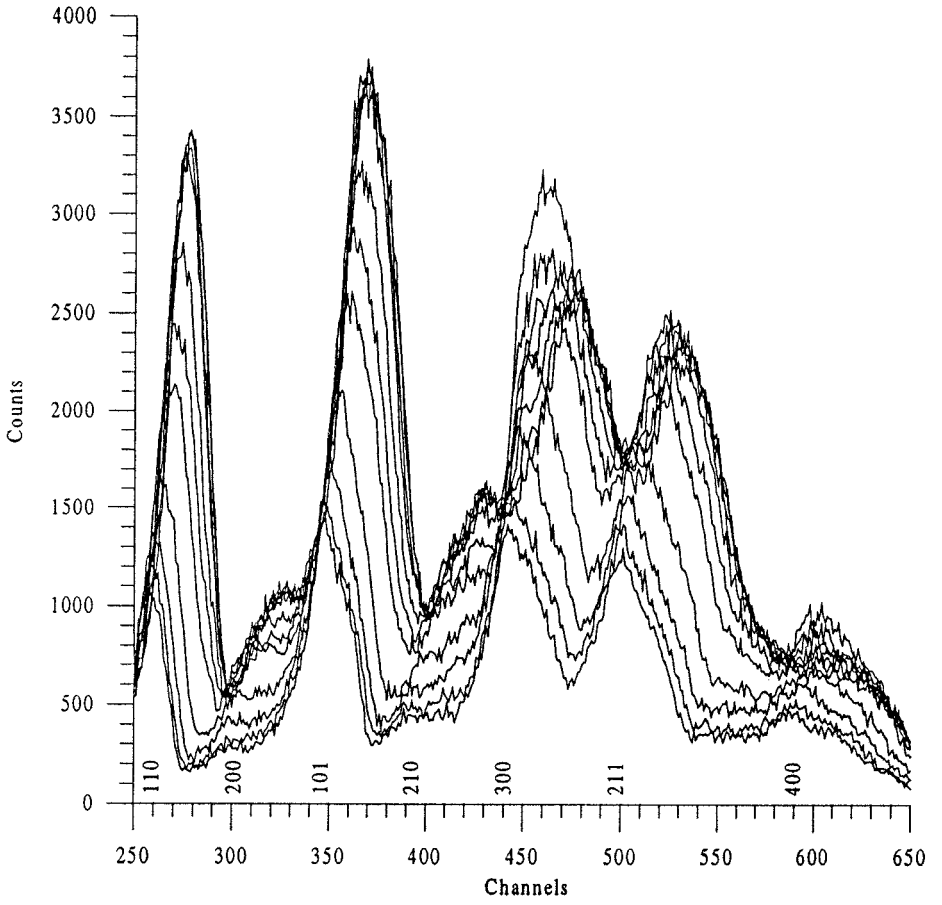

Figure 26. X-ray diffraction pattern collected using the prototype of the energy-dispersive diffractometer, collected from 24 °C (bottom) to 600 °C (top) during the heating process. (Reprinted with permission from [35]; copyright 1995 by The American Institute of Physics.)

structure of a membrane induced by the insertion of DHPs as doping substances. The effects of the insertions of the two drugs on the diffraction peak intensities are shown in figure 27.

In both cases the peak intensities decrease with increasing drug concentration, although the effect is faster for lacidipine than for nifedipine. Then, a kinetic study was performed to investigate the influence of the DHP doping on the phase transition temperature of the chains forming the membrane. Unlike the usual isothermal measurements to obtain $x(t)$, in this case, slow heating of the sample was carried out while its diffraction spectra were being collected (200 s each). The initial and the final spectra at 16 and 26 °C are given in figure 28. This route represents a useful alternative when just the transition temperature is sought.

Also in this measurement an effect of the introduction of the two drugs can be noted (figure 29). The transition occurs at about 23 °C for the undoped membrane. The temperature decreases when the sample is doped with nifedipine, while the doping with lacidipine does not seem to affect it. The conclusion is that lacidipine left part of the bilayer unaffected by its insertion, creating another phase that involves only the

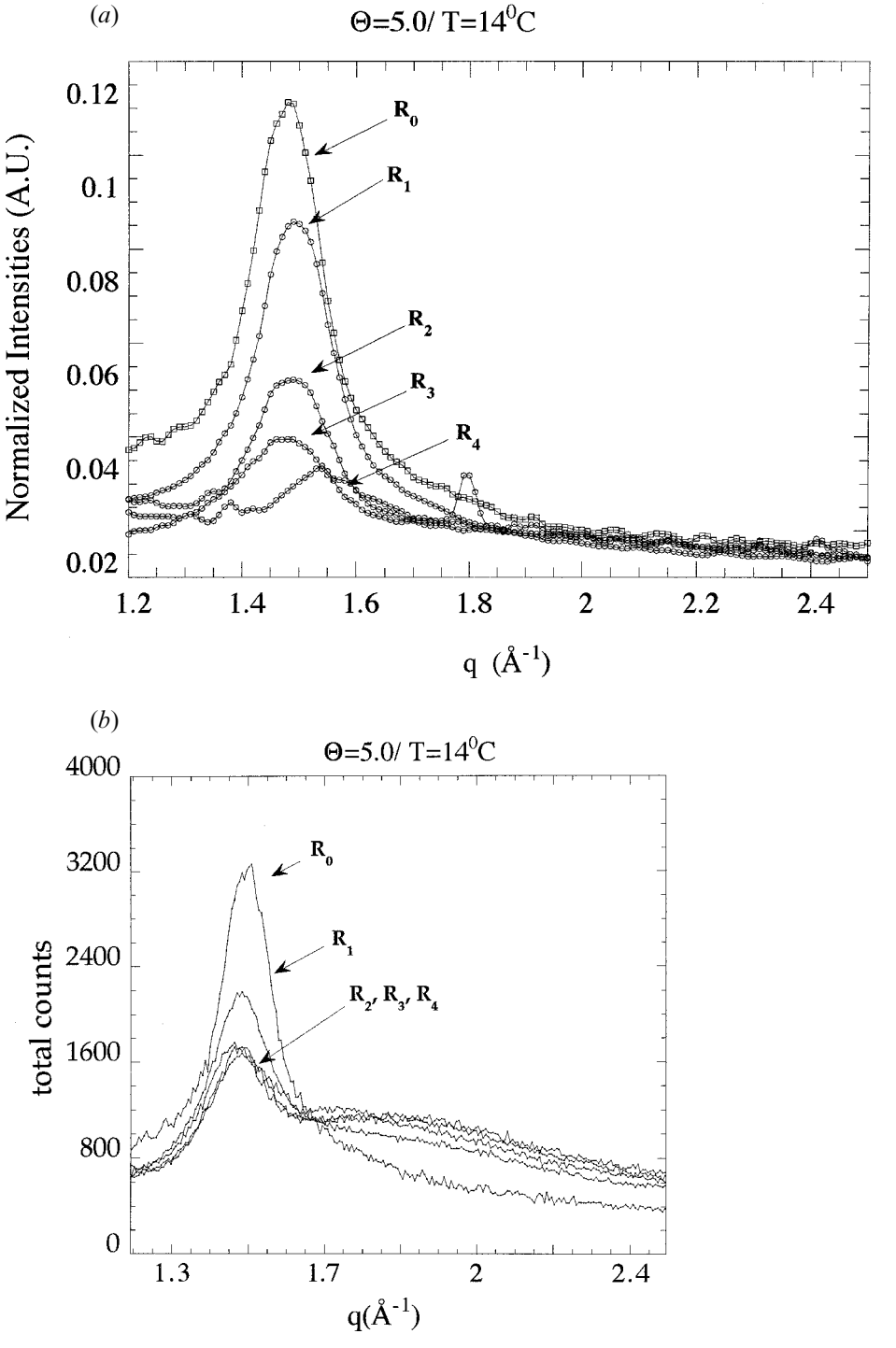

Figure 27. The effect of the interaction of the two DHPs on the diffraction peak due to the DMPC bilayer's acyl-chain distances (all spectra have been acquired for 1000 s). (*a*) Nifedipine at different molar ratios of DHP to DMPC: $R_0 = 0$; $R_1 = 4\times10^{-4}$; $R_2 = 4\times10^{-3}$; $R_3 = 6\times10^{-3}$; $R_4 = 5\times10^{-1}$. The spectra are normalized at the DMPC

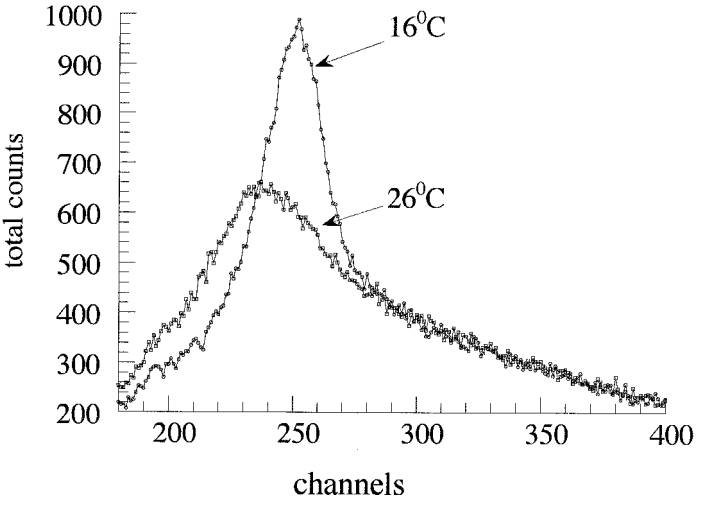

Figure 28. DMPC diffraction spectra at two different temperatures before and after the PT. The main peak corresponds to the quasicrystalline PB´ phase; the lower peak corresponds to the liquid-like (amorphous) Lα phase. (Reprinted with permission from [39]; copyright 1998 by Elsevier Science B.V.)

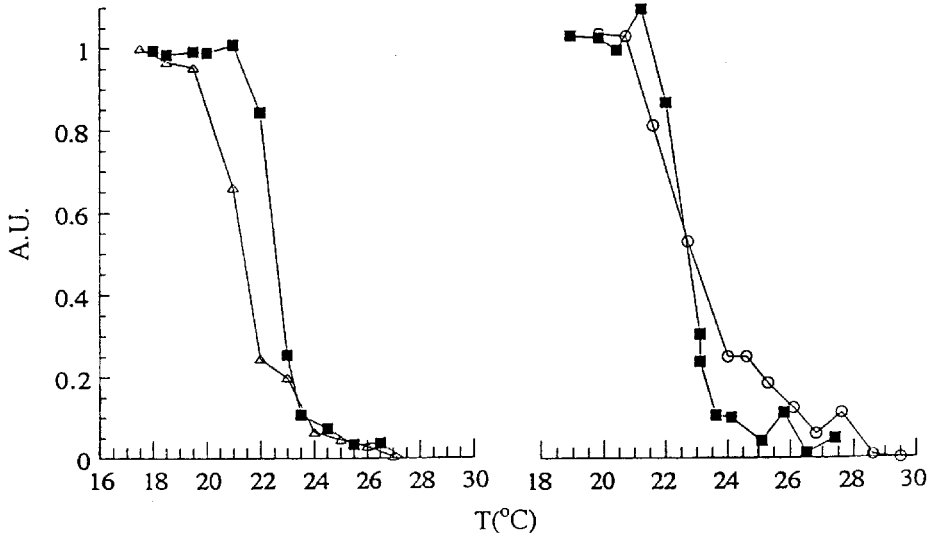

Figure 29. The integral value of a spectral region (1.40 Å^{-1} < q < 1.55 Å^{-1}) of the diffraction spectra shown in figure 28 against temperature, where the P_B–Lα PT occurs at the following temperatures: (■), 22.8 °C, DMPC pure sample; (○), 22.8 °C, lacidipine-doped DMPC sample; (△), 21.5 °C, nifedipine-doped DMPC sample. For each doped sample kinetic a pure DMPC transition has been performed. (Reprinted with permission from [39]; copyright 1998 by Elsevier Science B.V.)

---

concentration. (*b*) Lacipidine at different molar ratios of DHP to DMPC: $R_0 = 0$; $R_1 = 10^{-4}$; $R_2 = 4\times10^{-3}$; $R_3 = 10^{-2}$; $R_4 = 5\times10^{-1}$. (Reprinted with permission from [39]; copyright 1998 by Elsevier Science B.V.)

rest of lipids. In contrast, nifedipine molecules seem to be distributed randomly inside the bilayer, probably creating aggregates in the hydrophobic region.

References

[1] Schwartz, L. H., and Cohen, J. B., 1987, *Diffraction from Materials* (Berlin: Springer Verlag), p. 46.
[2] Murata, Y., and Nishikawa, K., 1978, *Bull. chem. Soc. Japan*, **51**, 411.
[3] James, R. W., 1982, *The Optical Principles of the Diffraction of X-rays* (Woodbridge, Connecticut: Ox-Bow Press), p. 464.
[4] Giessen, B. C., and Gordon, G. E., 1968, *Science*, **159**, 973.
[5] Prober, J. M., and Schultz, J., 1975, *J. appl. Crystallogr.*, **8**, 405.
[6] Egami, T., 1978, *J. Mater. Sci.*, **13**, 2587.
[7] Nishikawa, K., and Iijima, T., 1984, *Bull. chem. Soc. Japan*, **57**, 1750.
[8] Caminiti, R., Sadun, C., Rossi Albertini, V., Cilloco, F., and Felici, R., 1991, *Proceedings of the 25th National Congress of Physical Chemistry*, Cagliari, Italy, 17–21 June 1991; 1993, It. Pat. 01261484.
[9] *International Tables of X-ray Crystallography*, 1974 (Birmingham, UK: Kynoch Press).
[10] Jackson, J. D., 1975, *Classical Electrodynamics* (New York: Wiley).
[11] Rossi Albertini, V., Bencivenni, L., Caminiti, R., Cilloco, F., and Sadun, C., 1996, *J. macromol. Sci.—Phys.* B, **35**, 199.
[12] Rossi Albertini, V., Caminiti, R., Cilloco, F., Croce, F., and Sadun, C., 1997, *J. macromol. Sci.—Phys.* B, **36**, 221.
[13] Nishikawa, K., and Murata, Y., 1979, *Bull. chem. Soc. Japan*, **52**, 293.
[14] Nishikawa, K., and Kitagawa, N., 1980, *Bull. chem. Soc. Japan*, **53**, 2804.
[15] Nishikawa, K., 1986, *Bull. chem. Soc. Japan*, **59**, 2920.
[16] Nishikawa, K., and Iijima, T., 1988, *Bull. chem. Soc. Japan*, **61**, 217.
[17] Nishikawa, K., and Iijima, T., 1990, *J. phys. Chem.*, **94**, 6227.
[18] Hosokawa, S., Matsuoka, T., and Tamura, K., 1991, *J. phys.: condens. Matter*, **3**, 4443.
[19] Okhulkov, U. A. V., Demianets, Yu. N., and Gorbaty, Yu. E., 1994, *J. phys. Chem.* **100**, 1578.
[20] Meloni, S., Pieretti, A., Bencivenni, L., Albertini, V., Sadun, C., and Caminiti, R., 1999, VIII Workshop on Computational Materials Science 18–22 September 1996, S. Margherite di Pule (CA), Italy (to be published).
[21] Caminiti, R., Carbone, M., Panero, S., and Sadun, C., 1999 (to be published).
[22] Gontrani, L., Caminiti, R., Bencivenni, L., and Sadun, C., 1999, *Chem. Phys. Lett.* **301**, 131.
[23] Fritsch, G., and Wagner, C. N. J., 1986, *Z. Phys.* B, **62**, 189.
[24] McKeown, D. A., 1987, *Phys. Chem. Glasses*, **28**, 156.
[25] Capobianchi, A., Paoletti, A. M., Pennesi, G., Rossi, G., Caminiti, R., and Ercolani, C., 1994, *Inorg. Chem.*, **33**, 4635.
[26] Capobianchi, A., Paoletti, A. M., Pennesi, G., Rossi, G., Caminiti, R., Sadun, C., and Ercolani, C., 1996, *Inorg. Chem.*, **35**, 4643.
[27] Atzei, D., Filippo, D. De, Rossi, A., Caminiti, R., and Sadun, C., 1995, *Spectrochim. Acta* A, **51**, 11.
[28] Atzei, D., Filippo, D. De, Rossi, A., Caminiti, R., and Sadun, C., 1996, *Inorg. Chim. Acta*, **248**, 203.
[29] Caminiti, R., Carbone, M., Mancini, G., and Sadun, C., 1997, *J. mater. Chem.*, **7**, 1331.
[30] Carbone, M., Caminiti, R., and Sadun, C., 1996, *J. mater. Chem.*, **6**, 1709.
[31] Abis, L., Belli Dell' Amico, D., Busetto, C., Calderazzo, F., Caminiti, R., Ciofi, C., Garbassi, F., and Masciarelli, G., 1998, *J. mater. Chem.*, **8**, 751.
[32] Burragato, F., Caminiti, R., Ferraro, M., Gelli, J., and Sadun, C., 1997, *Fuel*, **76**, 887.
[33] Caminiti, R., Gleria, M., Lipkowitz, K. B., Lombardo, G. M., and Pappalardo, G. C., 1996, *J. Am. chem. Soc.*, **119**, 2196.
[34] Caminiti, R., D'Ilario, L., Martinelli, A., Piozzi, A., and Sadun, C., 1997, *Macromolecules*, **30**, 7970.
[35] Ballirano, P., Maras, A., Caminiti, R., and Sadun, C., 1995, *Powder Diffraction*, **10**, 173.

[36] CAMINITI, R., SADUN, C., BIONDUCCI, M., BUFFA, F., ENNAS, G., LICHERI, G., MUSINU, A., and NAVARRA, G., 1997, *Gazz. Chim. It.*, **127**, 59.
[37] ROSSI ALBERTINI, V., CAMINITI, R., CILLOCO, F., CROCE, F., and SADUN, C., 1997, *J. macromol. Sci.—Phys.* B, **36**, 623.
[38] ROSSI ALBERTINI, V., CAMINITI, R., and ISOPO, A., 1999, *J. macromol. Sci.—Phys.* B, **38**, 329.
[39] BOFFI, F., CAMINITI, R., SADUN, C., CAPUANI, S., GIOVANNELLI, A., and CONGIU CASTELLANO, A., 1998, *Chem. Phys. Lett.*, **286**, 473.
[40] SCROSATI, B., 1990, *Molec. Crystals liq. Crystals*, **190**, 161.
[41] ZALLEN, R., 1983, *The Physics of Amorphous Solids* (New York: Wiley–Interscience).
[42] FARRINGTON, G. C., and LINFORD, R. G., 1990, *Polymer Electrolyte Reviews*, Vol. 2, edited by McCallum and Vincent (London), p. 225.
[43] LINFORD, R. G., 1993, *Application of Electroactive Polymers*, edited by B. Scrosati (London: Chapman & Hall).
[44] CAPUANO, F., CROCE, F., PANERO, S., and SCROSATI, B., 1991, *J. electrochem. Soc.*, **138**, 418C.
[45] VINCENT, C. A., 1990, *Electrochemical Science and Technology of Polymers*, edited by Linford (London: Elsevier Applied Science).
[46] ZIABICKI, A., and ALFONSO, G. C., 1994, *Colloid Polym. Sci.*, **272**, 1027.
[47] ALFONSO, G. C., and ZIABICKI, A., 1995, *Colloid Polym. Sci.*, **273**, 317.
[48] SCOTT, M. G., 1983, *Amorphous Metallic Alloys*, edited by F. E. Luborsky (London: Butterworth), p. 144.
[49] KOSTER, U., and HEROLD, U., 1981, *Glassy Metals I*, edited by H. J. Guntherodt and H. Beck (Berlin: Springer), p. 225.
[50] GLAVEE, G. N., KLABUNDE, K. J., SORENSEN, C. M., and HADJAPANAYIS, G. C., 1992, *Langmuir*, **8**, 771.
[51] RANGANATHAN, S., and VON HEIMENDAHL, M., 1981, *J. Mater. Sci.*, **16**, 2401.
[52] GUNDY, H. D., and HASSAN, I., 1982, *Can. Mineral.*, **20**, 239.
[53] EMIRALIEV, A., and YAMZIN, I. I., 1982, *Soviet Phys. Crystallogr.*, **27**, 27.
[54] HASSAN, I., and BUSECK, P. R., 1992, *Can. Mineral.*, **22**, 341.
[55] JARCHOW, O., 1965, *Z. Kristallogr.*, **122**, 407.
[56] SMOLIN, Y. I., SHEPELEV, Y. F., BUTIKOVA, I. K., and KOBIAKOV, I. B., 1981, *Soviet Phys. Crystallogr.*, **26**, 33.
[57] RHODES, D. G., SARMIENTO, J. G., and HERBETTE, L. G., 1985, *Molec. Pharmacol.*, **27**, 612.
[58] GAMBALE, F., and DELLACASAGRANDE, F., 1994, *Cardioavasc. Pharmacol.*, **24**, 14.
[59] INOKO, Y., and MITSUI, T., 1978, *J. phys. Soc. Japan*, **44**, 1918.
[60] JANIAK, M., SMALL, D., and SHIPLEY, G., 1979, *J. biol. Chem.*, **254**, 6068.
[61] KNOLL, W., 1986, *Biochim. Biophys. Acta*, **863**, 329.